PATENT

IN THE UNITED STATES PATENT AND TRADEMARK OFFICE

Applicant	: Sean K. Lehman	Attorney Docket	: IL-10883
Serial No.	: 10/814,435	Art Unit	: 3737
Filed	: March 30, 2004	Examiner	: J. Lamprecht
For	: Radial Reflection Diffraction Tomography		

DECLARATION UNDER 37 CFR §1.131

Commissioner for Patents
P.O. Box 1450
Alexandria, VA 22313-1450

Dear Sir:

I, John P. Wooldridge, hereby declare that I am a citizen of the United States of America and a resident of Livermore, California.

I am a registered patent attorney, having USPTO registration number 38725 and have been registered since December 1994. I am a California licensed attorney, having California Bar no. 153511 and have been licensed as such since June 1991. I have a Juris Doctor Degree, a Degree in Laser Electro-Optics and have passed the engineer-in-training examination.

I have been in private practice as a patent attorney since the year 2000. I was a Patent Attorney/Assistant Laboratory Counsel at Lawrence Livermore National Laboratory at Livermore, California from 1992 to 2000. I was a laser technician/mechanical technician at LLNL from 1980 to 1992.

I have read the office action and would like the examiner to consider my comments.

The inventor conceived the invention at least as early as January 4, 2001, as shown in the attached paper from the invention bearing that date and further evidence in the attached annotated paper from the inventor dated which is prior to the effective date of Cespedes et al. (i.e., April 19, 2002).

The invention was conceived by Dr. Lehman at least as early as January 4, 2001 as shown in the attached document titled "Radial Reflection Diffraction Tomography for Intravascular Imaging." The attached paper from the inventor dated December 2, 2010 shows that the 2001 paper included sufficient detail that one skilled in the art could understand and reproduce the claimed invention. In the 2010 paper, footnote 1 shows that the term "Intravascular" implies imaging from within a blood vessel, i.e., an interspace. Footnote 2 shows that "diffraction tomography" is implicitly wave-based. Footnote 3 shows that IVUS operates by rotating an ultrasonic head. At each angular location, as the head rotates, it emits a field and collects the back-scattered energy. Footnote 4 shows that the term "back-scattered" implies reflection mode and reflected fields. Footnote 5 shows that the term "rotating" implies multiple angular locations. Footnote 6 shows that the term "wide-band" implies multiple frequencies. Footnote 7 shows that the term "frequency diversity" implies multiple frequencies. Footnote 8 shows that the term "multimonostatic" implies multiple spatial locations. Footnote 9 shows that the term "pulse" implies multiple frequencies. Footnote 10 shows the term "reconstructed" implies imaging. Footnote 11 shows that the images are a

function of radius, r', and angle, θ'. Accordingly, the annotated paper dated December 2, 2010 shows that the information provided in the original paper dated January 4, 2001 is sufficient for one skilled in the art to practice the claimed invention.

A timeline showing diligence is as follows.

The inventor submitted an invention disclosure on June 1, 2001 as shown in the attached Record of Invention.

A classification review was initiated on June 6, 2001 as shown in the attached letter to William Fritchie.

An analysis of the invention disclosure was made to determine patentabilty, marketability export control, U.S. preference/competitiveness, adverse affects on defense activities of the U.S. Note that numerous invention disclosures are under review simultaneously. After completion of the invention review, the REGENTS sent the attached letter dated September 12, 2002 to DOE, electing to retain title to the invention.

As shown in the attached letter dated September 12, 2002, a request was made to the LLNL Laboratory Counsel that a patent application be prepared and filed.

As shown in the attached letter dated October 15, 2002 from DOE to LLNL, DOE approved the request for election to retain title.

A request for a provisional application was made to the Laboratory Counsel, as shown in the email dated May 12, 2003.

Approval of the classification review was provided as shown on the attached letter on May 29, 2003

A provisional application was filed on May 30, 2003, as shown on the attached Express Mail Certificate and the attached extensive specification bearing the USPTO application number stamp. The specification includes the paper relied upon by the applicant to show prior conception. If provides additional documents as well.

The nonprovisional application was filed on March 30, 204, as shown on the attached Certificate of Mailing bearing that date.

LLNL only employs 3 or 4 in-house patent attorneys at any given time, including the relevant time period. Each attorney has more than a year's amount of invention disclosures awaiting them for patent application preparation. Therefore, it normally takes each attorney at least one year to prepare any given patent application.

Accordingly, the applicant has shown due diligence from prior to the reference to a constructive reduction to practice.

I hereby declare that all statements made herein of my own knowledge are true and that all statements made on information and belief are believed to be true; and further that these statements were made with the knowledge that willful false statements and the like so made are punishable by fine or imprisonment, or both, under Section 1001 of Title 18 of the United States Code, and that such willful false statements may jeopardize the validity of the application or any patent issued thereon.

Respectfully submitted,

/John P. Wooldridge #38,725/
John P. Wooldridge
Attorney for Applicant
Registration No. 38,725

Dated: December 27, 2010

Radial Reflection Diffraction Tomography for Intravascular Imaging

Sean K. Lehman

January 4, 2001

Abstract

Intravascular imaging provides a method for identifying potentially life threatening vulnerable plaque build up on the interior of blood vessel walls. In current acoustical imaging techniques, a catheter with a rotating ultrasound transducer is inserted into a blood vessel. The transducer launches a pulse and collects the reflected signals from the surrounding tissue. Current imaging systems use a B-scan mode, whereby images are formed from the envelope of the received signal and by assuming ray theory (geometrical optics). These images are not able to distinguish between vulnerable and stable plaque. Diagnosis of vulnerable plaque is of clinical importance because its tendency to detach from the vessel wall and cause a stroke.

We propose to develop a new imaging modality, diffraction tomography, to determine plaque structure using intravascular ultrasound (IVUS) probes. The technique will still make use of the back-scattered field received by the cylindrical IVUS probe. However, the technique will provide improved imaging capability because it will make use of both the phase and amplitude of the reflected signal and will properly account for the wave nature of the propagation. The technique is referred to as "radial reflection diffraction tomography" because of the radial configuration of the transducer and the tomographic paradigm is used to reconstruct the structure of the tissue from the reflected waves.

The proposed research will consist of theoretical, numerical and experimental components. The theoretical development of a tomographic algorithm for reflected signals in a radial geometry is an unsolved problem. A novel analytical approach will be developed to obtain a practical inversion scheme. Numerical calculations of the propagation problem will make

PERSONAL NOTES

use of expertise both at LLNL and BU to simulate ultrasound propagation through an inhomogeneous medium - for both the forward and backscattered waves. The numerical results will be used to assist in the development of the inversion procedure. The experimental component will be carried out at BU in the CenSSIS MedBED test system. A commercial IVUS probe will be used with either a tissue phantom or in vitro vessel preparation to obtain controlled and repeatable data sets with which to test the inversion algorithm.

The collaboration between LLNL and BU will bring together two groups with complementary expertise to attack the problem of vulnerable plaque. The goal will be to provide a unique approach to characterise the plaque; an approach with a firm theoretical basis that is grounded with results from simulations and experiments. The important societal problem of identifying vulnerable plaque will be advanced by this research.

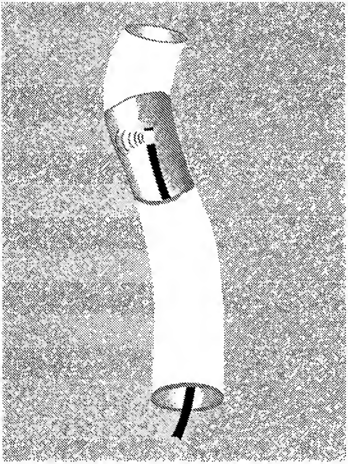

1 Statement of Problem

A rotating wide band transducer, located at the end of a catheter, is snaked into a tube.

The transducer collects reflection mode data at all planar angles at a fixed radius.

The goal is to develop a diffraction tomography imaging technique to reconstruct planar cross-slices of the material surrounding the tube.

Hence the name "radial reflection mode diffraction tomography."

Applications include

- Imaging of blood vessel walls;
- Imaging of specially prepared waste drums with inspection tubes inserted within them;
- The "pig" problem of natural gas and oil pipelines.

The motivation for this is improving current intravascular ultrasound imaging. A catheter is inserted into blood vessels and a rotating ultrasound transducer collects reflection data from the vessel wall. The current imaging technique performs B-scans of the vessel walls. B-scan theory is based upon Beer's law. I wish to extend the imaging technique using diffraction tomography which is based upon the wave equation. I anticipate enhancements in resolution and contrast.

2 Introduction

Operating conditions:

- Transducer rotates at a fixed radius, R_0, about the origin;
- Must use frequency diversity which implies an incident pulse;
- Multimonostatic mode;
- Reflection mode;
- Transducer emits a pulse and records the backscattered field;
- Geometry is that of Figure 2.
  The transducer is located at $\mathbf{r}_0 = R_0 \, (\cos\theta, \sin\theta)$.
  The observation point (to be reconstructed) is located at $\mathbf{r}' = r' \, (\cos\theta', \sin\theta')$.
  $R_0 < r'$.

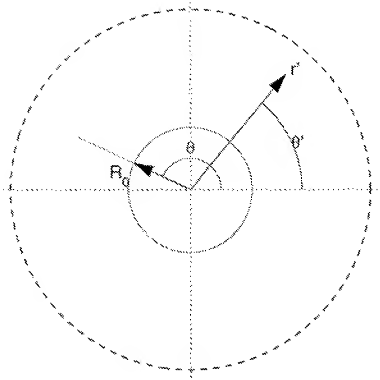

r'
θ'
θ
R_0

3 Derivation of Forward Model

Use as fundamental equation the Helmholtz equation,

$$\left[\nabla^2 + k^2(\mathbf{r})\right] u(\mathbf{r},\omega) \quad = \quad -p(\mathbf{r},\omega), \tag{1}$$

where

$\mathbf{r} \equiv (x,y) = (r,\theta)$	is the spatial coordinate,
ω	is the temporal frequency,
$k(\mathbf{r})$	is the wavenumber of the inhomogeneous medium surrounding the transducer,
$u(\mathbf{r},\omega)$	is the total field,
$p(\mathbf{r},\omega)$	is the incident pulse.

For convenience, drop the explicit ω dependence.

Add $k_0 u(r)$ to both sides of Eqn. 1 where $k_0 \equiv \omega/v_0$, and move the inhomogeneous term to the right hand side:

$$\left[\nabla^2 + k_0^2\right] u(\mathbf{r}) \quad = \quad -p(\mathbf{r}) - \left[k^2(\mathbf{r}) - k_0^2\right] u(\mathbf{r}). \tag{2}$$

Define the *object function* as

$$o(\mathbf{r}) \quad \equiv \quad \frac{k^2(\mathbf{r})}{k_0^2} - 1, \tag{3}$$

and express Eqn. 2 as

$$\left[\nabla^2 + k_0^2\right] u(\mathbf{r}) \quad = \quad -p(\mathbf{r}) - k_0^2 o(\mathbf{r}) u(\mathbf{r}). \tag{4}$$

We may use Green's theorem to cast the differential equation of Eqn. 4 into an integral equation,

$$u(\mathbf{r}) = \int d\mathbf{r}'\, G(\mathbf{r}-\mathbf{r}')\, p(\mathbf{r}') + k_0^2 \int d\mathbf{r}'\, G(\mathbf{r}-\mathbf{r}')\, o(\mathbf{r}')\, u(\mathbf{r}'), \qquad (5)$$

where we have ignored the boundary conditions and

$$G(\mathbf{r}-\mathbf{r}') = \begin{cases} \frac{i}{4}\, H_0^{(1)}(k_0\,|\mathbf{r}-\mathbf{r}'|) & n=2, \\ \\ \frac{1}{4\pi\,|\mathbf{r}-\mathbf{r}'|}\, e^{ik_0|\mathbf{r}-\mathbf{r}'|} & n=3. \end{cases} \qquad (6)$$

NOTE: Hankel function definition, $H_0^{(1)}(r) \equiv J_0(r) + iN_0(r)$.

The *primary source* is

$$u_i(\mathbf{r}) \equiv \int d\mathbf{r}'\, G(\mathbf{r}-\mathbf{r}')\, p(\mathbf{r}'), \qquad (7)$$

so that Eqn. 5 reads

$$u(\mathbf{r}) = u_i(\mathbf{r}) + k_0^2 \int d\mathbf{r}'\, G(\mathbf{r}-\mathbf{r}')\, o(\mathbf{r}')\, u(\mathbf{r}'). \qquad (8)$$

The *scattered field* is defined as

$$\begin{aligned} u_s(\mathbf{r}) &\equiv u(\mathbf{r}) - u_i(\mathbf{r}), \\ &= k_0^2 \int d\mathbf{r}'\, G(\mathbf{r}-\mathbf{r}')\, o(\mathbf{r}')\, u(\mathbf{r}'). \end{aligned} \qquad (9)$$

Let the measurement surface be at $\mathbf{r}_0 \equiv (R_0, \theta)$ for R_0 fixed and $0 \leq \theta < 2\pi$. Thus, the *measured scattered field* is

$$u_s(\mathbf{r}_0) \;=\; k_0^2 \int d\mathbf{r}'\, G(\mathbf{r}_0 - \mathbf{r}')\, o(\mathbf{r}')\, u(\mathbf{r}'). \tag{10}$$

Express $|\mathbf{r}_0 - \mathbf{r}'|$ in polar coordinates:

$$\begin{aligned}
|\mathbf{r}_0 - \mathbf{r}'|^2 &= (x_0 - x')^2 + (y_0 - y')^2 \\
&= (R_0 \cos\theta - r' \cos\theta')^2 + (R_0 \sin\theta - r' \sin\theta')^2 \\
&= R_0^2 + r'^2 - 2R_0 r' \cos(\theta - \theta').
\end{aligned} \tag{11}$$

Define

$$\boxed{R^2 \;\equiv\; R_0^2 + r'^2 - 2R_0 r' \cos(\theta - \theta').} \tag{12}$$

Thus, in polar coordinates, Eqn. 10 reads

$$\boxed{u_s(R_0, \theta) \;=\; k_0^2 \int r' dr' \int d\theta'\, G(R)\, o(r', \theta')\, u(r', \theta').} \tag{13}$$

Eqn. 13 is the forward model of the scattered field. No approximations have been made.

Let the incident field be a point source located at $\mathbf{r}_0$, obeying

$$\left[\nabla^2 + k_0^2\right] u_i(\mathbf{r}' - \mathbf{r}_0) \;=\; -A\,\delta(\mathbf{r}' - \mathbf{r}_0). \tag{14}$$

NOTE: A, the incident pulse amplitude is a function of ω, $A = A(\omega)$.
NOTE: Antenna characteristics are not modeled.

Thus, the incident field is

$$u_i(\mathbf{r}' - \mathbf{r}_0) \;=\; A\,G(R). \tag{15}$$

NOTE: $\mathbf{r}_0 = (R_0, \theta)$ for $0 \leq \theta < 2\pi$ is the location of the transceivers; $\mathbf{r}' = (r', \theta')$ for $r' > R_0$ and $0 \leq \theta' < 2\pi$ is the location of the observation point. In practice there are N_{trans} discrete transceiver locations. Thus, θ is a discretely index variable, θ_n where $n = 0, 1, \cdots, N_{trans} - 1$. Thus, Eqn. 13 represents a set of N_{trans} equations.

As is common, invoke the Born approximation,

$$o(\mathbf{r}) \;\equiv\; \frac{k^2(\mathbf{r})}{k_0^2} - 1 \;\approx\; 0, \tag{16}$$

replace the *total field* by the *incident field*, and express Eqn. 13 as

$$\boxed{u_s(R_0, \theta) \approx u_s^B(R_0, \theta) \;\equiv\; A k_0^2 \int r' dr' \int d\theta'\, G^2(R)\, o(r', \theta')} \tag{17}$$

Eqn. 17 serves as our *forward model*.

Now in two- and three-dimensions, we have

$$G(R) \;=\; \begin{cases} \dfrac{i}{4} H_0^{(1)}\left(k_0\sqrt{R_0^2 + r'^2 - 2R_0 r' \cos(\theta - \theta')}\right) & n = 2, \\[2ex] \dfrac{e^{ik_0(R_0^2 + r'^2 - 2R_0 r' \cos(\theta - \theta'))}}{4\pi\sqrt{R_0^2 + r'^2 - 2R_0 r' \cos(\theta - \theta')}} & n = 3. \end{cases} \tag{18}$$

NOTE: for $n = 3$, we have assumed all measurements are taken in the same plane so that $z - z' \equiv 0$.

Hankel function expansion from G&R (page 992):

$$\boxed{\begin{aligned} H_0^{(1)}(k_0R) &= \sum_{n=0}^{\infty}(2-\delta_{n0})\, J_n(k_0R_0)H_n^{(1)}(k_0r')\, \cos(n(\theta-\theta')) \\ &= \sum_{n=-\infty}^{\infty} J_n(k_0R_0)H_n^{(1)}(k_0r')\, e^{in(\theta-\theta')} \end{aligned}} \quad (19)$$

where and $R_0 < r'$.

From M&F page 888, or Morse & Ingard Eqn. 7.3.15:

$$\boxed{\begin{aligned} \frac{e^{ik_0R}}{R} &= i\sum_{n=0}^{\infty}(\delta_{0n}-2)\, \cos(n(\theta-\theta')) \times \\ & \qquad \int_0^{\infty} kdk\, J_n(kR_0)J_n(kr')\, \frac{e^{i\sqrt{k_0^2-k^2}|z-z'|}}{\sqrt{k_0^2-k^2}}. \end{aligned}} \quad (20)$$

For $z = z'$, we have

$$\boxed{\frac{e^{ik_0R}}{R} = i\sum_{n=0}^{\infty}(\delta_{0n}-2)\, \cos(n(\theta-\theta'))\int_0^{\infty} kdk\, \frac{J_n(kR_0)J_n(kr')}{\sqrt{k_0^2-k^2}}} \quad (21)$$

Recall some orthogonality relations...

$$\int_0^{2\pi} d\theta \, \cos(m\theta)\cos(n\theta) = \begin{cases} 2\pi\delta_{mn} & n = 0, \\ \pi\delta_{mn} & n \neq 0, \end{cases} \tag{22}$$

$$\int_{-1}^{1} dx \, P_m(x) P_n(x) = \frac{2\delta_{mn}}{2n+1}, \tag{23}$$

or

$$\int_0^{\pi} \sin\theta d\theta \, P_m(\cos\theta) P_n(\cos\theta) = \frac{2\delta_{mn}}{2n+1}. \tag{24}$$

$$\int_0^{2\pi} d\theta \, e^{i(m-n)\theta} = 2\pi \, \delta_{mn} \tag{25}$$

4 Inversion Process Using Two-Dimensional Green's Function

Substitute Eqn. 19 into Eqn. 17:

$$u_s^B(R_0,\theta) = -\frac{Ak_0^2}{16}\int r'dr'\int d\theta' \left[\sum_{n=-\infty}^{\infty} J_n(k_0R_0)H_n^{(1)}(k_0r')e^{in(\theta-\theta')}\right]^2 \times o(r',\theta') \tag{26}$$

$$= -\frac{Ak_0^2}{16}\sum_{m,n=-\infty}^{\infty} J_m(k_0R_0)J_n(k_0R_0)\, e^{i(m+n)\theta} \times \int r'dr'\int d\theta'\, H_m^{(1)}(k_0r')H_n^{(1)}(k_0r')\, e^{-i(m+n)\theta'}\, o(r',\theta') \tag{27}$$

Observations regarding Eqn. 27:

- We wish to solve for either the object or the object's spatial spectrum;
- We wish to develop a Fourier Diffraction Theorem for this geometry. This will tell us how the object's spatial spectrum is mapped within this measurement framework;
- We wish to "eliminate" the double summation;
- The spatial integration is less troublesome as this can lead to the Fourier transform of the object function.

Fourier transform Eqn. 27. Define

$$U_{sm'}^B(R_0) \equiv \int_0^{2\pi} d\theta\, u_s^B(R_0,\theta)\, e^{im'\theta}. \tag{28}$$

Multiply both sides of Eqn. 27 by $e^{im'\theta}$ and integrate over θ:

$$\begin{aligned} U^B_{sm'}(R_0) &= -\frac{Ak_0^2}{16} \sum_{m,n=-\infty}^{\infty} J_m(k_0R_0)J_n(k_0R_0) \left[\int_0^{2\pi} d\theta\, e^{i(m+n+m')\theta}\right] \times \\ &\quad \int r'dr' \int d\theta'\, H_m^{(1)}(k_0r')H_n^{(1)}(k_0r')\, e^{-i(m+n)\theta'}\, o(r',\theta') \end{aligned} \tag{29}$$

Use

$$\int_0^{2\pi} d\theta\, e^{i(m-n)\theta} = 2\pi\, \delta_{mn},$$

so that Eqn. 29 becomes

$$\begin{aligned} U^B_{sm'}(R_0) &= -\frac{\pi\, Ak_0^2}{8} \sum_{m,n=-\infty}^{\infty} J_m(k_0R_0)J_n(k_0R_0) \left[\delta_{n,-(m'+m)}\right] \times \\ &\quad \int r'dr' \int d\theta'\, H_m^{(1)}(k_0r')H_n^{(1)}(k_0r')\, e^{-i(m+n)\theta'}\, o(r',\theta') \qquad (30) \\ &= -\frac{\pi\, Ak_0^2}{8} \sum_{m=-\infty}^{\infty} J_m(k_0R_0)J_{-(m'+m)}(k_0R_0) \times \\ &\quad \int r'dr' \int d\theta'\, H_m^{(1)}(k_0r')H_{-(m'+m)}^{(1)}(k_0r')\, e^{im'\theta'}\, o(r',\theta') \qquad (31) \end{aligned}$$

Consider the double integral of Eqn. 31:

$$I = \int r' dr' \int d\theta' \, H_m^{(1)}(k_0 r') H_{-(m'+m)}^{(1)}(k_0 r') \, e^{im'\theta'} \, o(r', \theta'). \tag{32}$$

Replace $o(r', \theta')$ by its Fourier transform:

$$o(r', \theta') = \frac{1}{2\pi} \int dk_x \int dk_y \, O(k_x, k_y) \, e^{-i(k_x x' + k_y y')} \tag{33}$$

$$= \frac{1}{2\pi} \int dk_x \int dk_y \, O(k_x, k_y) \, e^{-ir'(k_x \cos\theta' + k_y \sin\theta')}. \tag{34}$$

Then Eqn. 32 reads,

$$\begin{aligned} I = & \frac{1}{2\pi} \int dk_x \int dk_y \, O(k_x, k_y) \times \\ & \int r' dr' \int d\theta' \, H_m^{(1)}(k_0 r') H_{-(m'+m)}^{(1)}(k_0 r') \times \\ & e^{im'\theta'} \, e^{-ir'(k_x \cos\theta' + k_y \sin\theta')}, \end{aligned} \tag{35}$$

$$\begin{aligned} = & \frac{1}{2\pi} \int dk_x \int dk_y \, O(k_x, k_y) \times \\ & \int r' dr' \, H_m^{(1)}(k_0 r') H_{-(m'+m)}^{(1)}(k_0 r') \times \\ & \int d\theta' \, e^{im'\theta'} \, e^{-ir'(k_x \cos\theta' + k_y \sin\theta')}, \end{aligned} \tag{36}$$

4.1 Method 1 for Inversion

Summarizing, we have

$$
\begin{aligned}
U^{B}_{mm'}(R_0) &= -\frac{\pi\, A k_0^2}{8} \sum_{m=-\infty}^{\infty} J_m(k_0 R_0) J_{-(m'+m)}(k_0 R_0) \times \\
&\int r' dr' \int d\theta'\, H^{(1)}_m(k_0 r') H^{(1)}_{-(m'+m)}(k_0 r')\, e^{im'\theta'}\, o(r', \theta') \quad (37) \\
&= -\frac{\pi\, A k_0^2}{8} \int r' dr' \int d\theta'\, o(r', \theta') \times \\
&\underbrace{\sum_{m=-\infty}^{\infty} J_m(k_0 R_0) J_{-(m'+m)}(k_0 R_0)\, H^{(1)}_m(k_0 r') H^{(1)}_{-(m'+m)}(k_0 r')\, e^{im'\theta'}}_{\text{Need a summation formula}} \quad (38)
\end{aligned}
$$

4.2 Method 2 for Inversion

Summarizing, we have

$$\begin{aligned} U^{B}_{sm'}(R_0) &= -\frac{\pi A k_0^2}{8} \sum_{m=-\infty}^{\infty} J_m(k_0 R_0) J_{-(m'+m)}(k_0 R_0) \times \\ & \int r' dr' \int d\theta' \, H^{(1)}_m(k_0 r') H^{(1)}_{-(m'+m)}(k_0 r') \, e^{im'\theta'} \, o(r', \theta'). \end{aligned} \quad (39)$$

Define

$$\begin{aligned} V_{mm'} &= \int r' dr' \int d\theta' \, H^{(1)}_m(k_0 r') H^{(1)}_{-(m'+m)}(k_0 r') \, e^{im'\theta'} \, o(r', \theta') \\ &= \int r' dr' \, H^{(1)}_m(k_0 r') H^{(1)}_{-(m'+m)}(k_0 r') \, \underbrace{\int d\theta' \, o(r', \theta') \, e^{im'\theta'}}_{\equiv O_{m'}(r')} \\ &= \underbrace{\int r' dr' \, H^{(1)}_m(k_0 r') H^{(1)}_{-(m'+m)}(k_0 r') \, O_{m'}(r')}_{\text{Use orthogonality relation}} \end{aligned} \quad (40)$$

So Eqn. 39 reads

$$U^{B}_{sm'}(R_0) = -\frac{\pi A k_0^2}{8} \sum_{m=-\infty}^{\infty} J_m(k_0 R_0) J_{-(m'+m)}(k_0 R_0) \, V_{mm'} \quad (41)$$

Solve Eqn. 41 for $V_{mm'}$ in terms of the known measured scattered field transform, $U^{B}_{sm'}(R_0)$. Then solve Eqn. 40 for $O_{m'}(r')$ in terms of $V_{mm'}$.

Response to IL-10883 Radial Reflection Diffraction Tomography Challenges

Sean K. Lehman

December 02, 2010

Abstract

Intravascular [1] imaging provides a method for identifying potentially life threatening vulnerable plaque build up on the interior of blood vessel walls. In current acoustical imaging techniques, a catheter with a rotating ultrasound transducer is inserted into a blood vessel. The transducer launches a pulse and collects the reflected signals from the surrounding tissue. Current imaging systems use a B-scan mode, whereby images are formed from the envelope of the received signal and by assuming ray theory (geometrical optics). These images are not able to distinguish between vulnerable and stable plaque. Diagnosis of vulnerable plaque is of clinical importance because its tendency to detach from the vessel wall and cause a stroke.

We propose to develop a new imaging modality, diffraction tomography [2], to determine plaque structure using intravascular ultrasound (IVUS) [3] probes. The technique will still make use of the back-scattered [4] field received by the cylindrical IVUS probe. However, the technique will provide improved imaging capability because it will make use of both the phase and amplitude of the reflected signal and will properly account for the wave nature of the propagation. The technique is referred to as "radial reflection diffraction tomography" because of the radial configuration of the transducer and the tomographic paradigm is used to reconstruct the structure of the tissue from the reflected waves.

[1] "Intravascular" implies imaging from within a blood vessel. I take this to be an interspace.

[2] "Diffraction tomography" is implicitly wave-based.

[3] IVUS operates by rotating an ultrasonic head. At each angular location, as the head rotates, it emits a field and collects the back-scattered energy.

[4] "Back-scattered" implies reflection mode and reflected fields.

The proposed research will consist of theoretical, numerical and experimental components. The theoretical development of a tomographic algorithm for reflected signals in a radial geometry is an unsolved problem. A novel analytical approach will be developed to obtain a practical inversion scheme. Numerical calculations of the propagation problem will make use of expertise both at LLNL and BU to simulate ultrasound propagation through an inhomogeneous medium - for both the forward and backscattered waves. The numerical results will be used to assist in the development of the inversion procedure. The experimental component will be carried out at BU in the CenSSIS MedBED test system. A commercial IVUS probe will be used with either a tissue phantom or in vitro vessel preparation to obtain controlled and repeatable data sets with which to test the inversion algorithm.

The collaboration between LLNL and BU will bring together two groups with complementary expertise to attack the problem of vulnerable plaque. The goal will be to provide a unique approach to characterize the plaque: an approach with a firm theoretical basis that is grounded with results from simulations and experiments. The important societal problem of identifying vulnerable plaque will be advanced by this research.

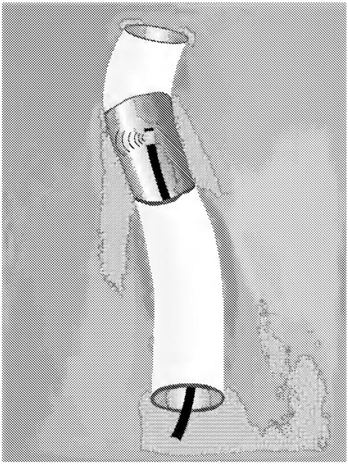

1 Statement of Problem

A rotating [5] wide band transducer [6], located at the end of a catheter, is snaked into a tube.

The transducer collects reflection mode data at all planar angles at a fixed radius.

The goal is to develop a diffraction tomography imaging technique to reconstruct planar cross-slices of the material surrounding the tube.

Hence the name "radial reflection mode diffraction tomography."

Applications include

- Imaging of blood vessel walls;
- Imaging of specially prepared waste drums with inspection tubes inserted within them;
- The "pig" problem of natural gas and oil pipelines.

The motivation for this is improving current intravascular ultrasound imaging. A catheter is inserted into blood vessels and a rotating ultrasound transducer collects reflection data from the vessel wall. The current imaging technique performs B-scans of the vessel walls. B-scan theory is based upon Beer's law. I wish to extend the imaging technique using diffraction tomography which is based upon the wave equation. I anticipate enhancements in resolution and contrast.

[5] "Rotating" implies multiple angular locations.

[6] "Wide band" implies multiple frequencies.

2 Introduction

Operating conditions:

- Transducer rotates at a fixed radius, R_0, about the origin;
- Must use frequency diversity [7] which implies an incident pulse;
- Multimonostatic mode [8];
- Reflection mode;
- Transducer emits a pulse [9] and records the backscattered field;
- Geometry is that of Figure 2.
  The transducer is located at $\mathbf{r}_0 = R_0\,(\cos\theta, \sin\theta)$.
  The observation point (to be reconstructed [10]) is located at $\mathbf{r}' = r'\,(\cos\theta', \sin\theta')$ [11].
  $R_0 < r'$.

[7] "Frequency diversity" implies multiple frequencies.

[8] "Multimonostatic" implies multiple spatial locations. Represented here by the different angular locations.

[9] "Pulse" implies multiple frequencies.

[10] That is, to be imaged.

[11] The images are a function of radius, r', and angle, θ'.

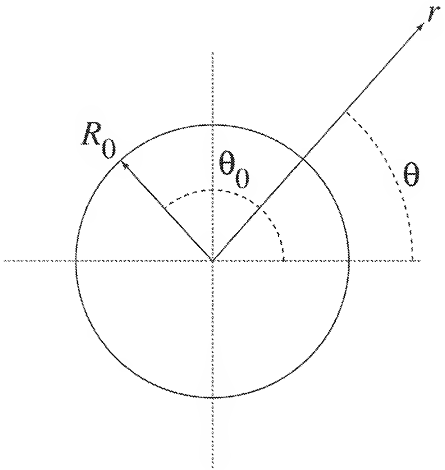

r
R_0
θ_0
θ

University of California
Lawrence Livermore
National Laboratory

RECEIVED

JUN 1 2001

LLNL-I.P.L.G.

RECORD OF INVENTION

LLNLFile No. IL-10883

This invention was made in the course of or under prime Contract No. W-7405-ENG-48 between the U.S. Department of Energy and the University of California. This Record of Invention is prepared for the Office of the Assistant General Counsel for Patents, U.S. Department of Energy.

I. Title of the Invention

Radial Reflection Diffraction Tomography

II. Inventor(s): those who conceived the invention

LLNL Inventor(s) (First, Middle, Last)	Title/Position	Directorate	Payroll Acct	Phone Number	Mail Stop
Sean K. Lehman	Engineer	EE/DSED	9784	3-3580	154

Non-LLNL Inventor(s) (F M L)	Title/Position	Employer	Phone Number	Fax Number	Subcontract #

III. Abstract of the Invention

This is a new application of diffraction tomography to an annular, outward-looking geometry. An annular array of transducers, or a single or pair of co-located transducers, either electromagnetic or acoustic, directed radially outward, launch a pulse and record the reflected backscattered field. The measured backscattered field is then used in a diffraction tomography reconstruction algorithm to create an image of the material or structure surrounding the transducers.

A diffraction tomographic imaging algorithm has never been developed for this geometry.

The transducers can be located at the end of a catheter which is inserted or "snaked" into an object or part under evaluation.

IV. Uses of the Invention (List past uses, current uses and potential uses for your invention)

LLNL or Government uses or possibilities for use:

- Bore hole tomographic imaging;
- Nondestructive evaluation (NDE) applications such as weapon or material part imaging.

Commercial or other uses or possibilities for use:

- Medical applications such as intravascular ultrasound (IVUS) imaging of blood vessel walls; intestine; prostate.

LLNL File No.

V. Keywords for Searches

A. Potential Licensees: list keywords for appropriate companies to contact concerning your invention.
• Medical equipment manufacturers (see IVUS systems, prostate imaging systems)
• Geophysical companies (bore hole tomography)

B. Patent search: list keywords for an effective patent search.
• Diffraction tomography, radial geometry, reflection mode, outward-looking.

VII. Background of the Invention

Please describe the background of the invention: what is the technical problem addressed by the invention and what solutions have been used in the past by others (successfully or unsuccessfully).

Intravascular ultrasound (IVUS) imaging provides a method for imaging the interior of blood vessel walls. In standard acoustical imaging techniques, a catheter with a rotating ultrasound transducer is inserted into a blood vessel. The transducer launches a pulse and collects the reflected signals from the surrounding tissue. Current imaging systems use a B-scan mode, whereby images are formed from the envelope of the received signal and by assuming straight ray theory (geometrical optics). These images suffer from the consequences of ray theory of sound propagation which does not model its wave nature.

I propose to develop a new imaging algorithm using diffraction. The technique will still make use of the backscattered field received by current cylindrical IVUS probes. However, because this technique will process both the phase and amplitude of the reflected signal and will properly account for the wave nature of the propagation, it can provide imagery with superior resolution and contrast of both the absorption and sound speed over that provided by existing IVUS systems. The technique is referred to as "radial reflection diffraction tomography" (RRDT) because of the radial configuration of the transducer and the tomographic paradigm used to reconstruct the structure of the tissue from the reflected waves.

The Center for Subsurface Sensing and Imaging Systems (CenSSIS) is a National Science Foundation (NSF) engineering research center headquartered at Northeastern University in Boston, MA. LLNL is a Strategic Affiliate of CenSSIS. Northeastern University, Boston University, and LLNL have applied as CenSSIS members to NSF for funding to develop RRDT into the next generation of

IVUS systems. We will have support from the Massachusetts General Hospital (MGH), and the medical equipment manufacturers of Boston Scientific and Analogic to build a prototype device.

University of California
Lawrence Livermore National Laboratory
Intellectual Property Law Group

June 6, 2001

IN STRICT CONFIDENCE
ATTORNEY WORK PRODUCT

Mail Station: L-703

Extension: 3-9034

Interoffice Memorandum

TO: **William Fritchie, L-302**

FROM: **Kathy Raymond**

SUBJECT: **New Disclosure and Record of Invention (ROI)**
LLNL Case No.: IL-10883
"Radial Reflection Diffraction Tomography"

Please review the attached disclosure for classification purposes only. As usual, when you have finished your review, sign the disclosure and return to me at L-703.

Thank you for your assistance, it is greatly appreciated.

Kathy Raymond

Kathy Raymond
Intellectual Property Law Group

Enclosure

Lawrence Livermore National Laboratory
Industrial Partnerships & Commercialization

September 12, 2002

Mr. William C. Daubenspeck
Office of Patent Counsel
U.S. Department of Energy
Oakland Operations Office
P.O. Box 808, L-376
Livermore, CA 94550

Subject: NOTICE OF ELECTION TO RETAIN TITLE TO DEFENSE PROGRAM INVENTION UNDER CLASS WAIVER W(C)-92-002

Dear Mr. Daubenspeck:

Pursuant to the terms of Contract W-7405-ENG-48 between the Department of Energy (DOE) and the Regents of the University of California (University), and subject to Class Waiver W(C)-92-002, we submit an Election Memorandum for the following invention:

DOE Case No. S-97,386
LLNL Docket No. IL-10883
Radial Reflection Diffraction Tomography
Inventor: Sean K. Lehman

The University has reviewed the subject invention disclosure with respect to: (1) export control; (2) United States preference/competitiveness; and (3) adverse impact upon the Naval Nuclear Propulsion Program and other nuclear and/or atomic energy defense activities of the Department of Energy and agrees to comply with all statutes and regulations governing export control, U.S. preference/competitiveness, and the Naval Nuclear Propulsion Program, et al., in dealing with the subject inventions. (A copy of the Invention Disclosure including a Classification Review, and an original signed Export Control Review for Licensing and Patents form, are attached to the enclosed Election Memorandum.)

Further, the University agrees to comply with Clause 66.1.F governing technology transfer activities under Contract Number W-7405-ENG-48.

Your prompt review of this Election Memorandum will be appreciated.

Sincerely,

Kathy Kaufman
for Karena McKinley
Director, Industrial Partnerships
& Commercialization

cc: Sean K. Lehman, L-154
Paul R. Martin, L-795
Janet G. Tulk, L-703

University of California, P.O. Box 808, L-795, Livermore, California 94551
University of California, 7000 East Avenue, L-795, Livermore, California 94551
Telephone (925) 422-6416; Facsimile (925) 423-8988; Email: ipandc@llnl.gov

Lawrence Livermore National Laboratory

Industrial Partnerships & Commercialization

September 12, 2002

Janet G. Tulk
Laboratory Counsel
LLNL, L-703

Subject: DOE Case No. S-97,386
LLNL Docket No. IL-10883
Invention Title: Radial Reflection Diffraction Tomography
Inventor: Sean K. Lehman

Dear Ms. Tulk:

This letter is to request that you prepare and file a U.S. patent application for the above-referenced matter on behalf of The Regents of the University of California. A waiver concerning the subject invention has been prepared and is being submitted to DOE OAK. A copy is enclosed for your file. Foreign filing is not requested at this time but will be revisited at a future date. We ask that your office track the foreign file date(s) and keep us accordingly advised.

Please proceed with this application for filing with the U.S. Patent Office in a timely manner.

Please send a copy of the patent application as filed, serial number, and filing data as they become available to Nina Rhodes and keep her advised regarding the progress of the filing.

At this time I ask that your office track the patent filing fees and prosecution costs for the subject application and keep our office informed of the expenditures required.

Sincerely,

for Kathy Kaufman

Karena McKinley
Director, Industrial Partnerships &
Commercialization

Attachment
cc: Sean K. Lehman, L-154
Paul R. Martin, L-795

University of California, P.O. Box 808, L-795, Livermore, California 94551
University of California, 7000 East Avenue, L-795, Livermore, California 94551
Telephone (925) 422-6416; Facsimile (925) 423-8988; Email: ipandc@llnl.gov

Department of Energy
National Nuclear Security Administration
Office of Chief Counsel
Intellectual Property Law Division

Livermore Office
P.O. Box 808, L-376
Livermore, CA 94550
(925) 422-4267
FAX (925) 422-8228

October 15, 2002

RECEIVED
OCT 1 6 2002
LLNL-I.P.L.G.

Karena D. McKinley
Director, Industrial Partnership and Commercialization
Lawrence Livermore National Laboratory, L-795
c/o Sara Sanders, LLNL-TTIP, L-795

Re: Approval of Election by LLNL under DOE Waiver W(C) 92-002-923
DOE Inven. Case No.: S-97,386
LLNL Inven. Docket No.: IL-10883
Inventor(s): Sean K. Lehman
Invention Title: Radial Reflection Diffraction Tomography

Dear Ms. McKinley:

Enclosed with this letter is a copy of the LLNL Election Memorandum for the above-identified invention. It has the signatures of the appropriate DOE officials approving LLNL's election. The effective date of DOE's approval is October 1, 2002.

Please have the LLNL Patent Group forward to this office a copy of each patent application filed on the referenced invention and a copy of any issued patents thereon.

Furthermore, have LLNL's Industrial Partnerships and Commercialization Program periodically provide this office with information demonstrating LLNL's commercialization efforts for the subject invention as required by Contract No. W-7405-ENG-48.

Respectfully,

William C. Daubenspeck
Patent Attorney

Enclosure

Copy to: Michael A. Wahlig, DOE-OAK, L-293 (w/o encl)
Janet G. Tulk, LLNL, L-703
Sean K. Lehman, LLNL, L-154 (w/o encl)

WCD:wkc

University of California
Lawrence Livermore National Laboratory

Classification Review of Patent Application

Docket Number:	IL-10883
Unclassified Title: (U)	**Radial Reflection Diffraction Tomography**
Inventors:	Sean Lehman

Authorized Derivative Classifier Determination

- ☒ **Unclassified**
- ☐ Unclassified, but Controlled
- ☐ UCNI Other:
- ☐ UCNI Reviewing Official Determination is required
- ☐ **Classified** - Level and Category

Specify Authority (Guide/Topics): 402.1, 402.2, 402.3

If NSI, Review/Declassify on (Date or Event):

Additional markings Required: Weapon Data - Sigma(s):

Other:

ADC Name: DAVID GOERZ	ADC Title: SPECIAL PROJECTS GL
ADC Signature: David Goerz	Date: 5/29/03

UCNI Reviewing Official Determination (If requested)

- ☐ The application does *not* contain UCNI.
- ☐ The application *may* contain UCNI.
- ☐ The application *does* contain UCNI.

Reviewing Official Signature:	Date

Classification Office Confirming Review

- ☒ The ADC's determination is correct. CG-DAA-2 / 402.1, 402.2, 402.3
- ☐ The Inventor's determination is correct.

The correct classification is:

Reviewing Official Signature: W. Fritchie	Date MAY 30 2003

William R. Fritchie
Classification/Export Control Adviser

Please type a plus sign (+) inside this box [+]

jc892 U.S. PTO

6/3/03 60/474861 . 053003

PTO/SB/16 (2-98)

Approved for use through 01/31/2001. OMB 0651-0037

Patent and Trademark Office, U.S. DEPARTMENT OF COMMERCE

Under the Paperwork Reduction Act of 1995, no persons are required to respond to a collection of information unless it displays a valid OMB control number.

PROVISIONAL APPLICATION FOR PATENT COVER SHEET

05/30/03 This is a request for filing a PROVISIONAL APPLICATION FOR PATENT under 37 CFR 1.53 (c).

A/ PROV

16447 U.S. PTO 60/474861 05/30/03

INVENTOR(S)

Given Name (first and middle [if any])	Family Name or Surname	Residence City and either State or Foreign Country
Sean K.	Lehman	Pleasanton, CA

☐ Additional inventors are being named on the separately numbered sheets attached hereto

TITLE OF THE INVENTION (280 characters max)

Radial Reflection Diffraction Tomography

Direct all correspondence to: **CORRESPONDENCE ADDRESS**

OR ☒ Customer Number 24981

Type Customer Number here

Place Customer Number Bar Code Label here

☒ Firm *or* Individual Name	Michael C. Staggs				
Address	Lawrence Livermore National Laboratory				
Address	P.O. Box 808, L-703				
City	Livermore	State	CA	Zip	94551
Country	US	Telephone	(925) 422-3682	Fax	(925) 423-2231

ENCLOSED APPLICATION PARTS (*check all that apply*)

☒ Specification Number of Pages: 39

☒ Drawing(s) Number of Sheets: included

☒ Other (specify): Express Mail Certificate; Return Postcard

METHOD OF PAYMENT OF FILING FEES FOR THIS PROVISIONAL APPLICATION FOR PATENT (*check one*)

☐ A check or money is enclosed to cover the filing fees

☒ Small Entity Statement on file

☒ The commissioner is hereby authorized to charge filing fees or credit any overpayment to Deposit Account Number: 12-0695

FILING FEE AMOUNT ($): 160.00

The invention was made by an agency of the United States Government or under a contract with an agency of the United States Government.

☐ No.

☒ Yes, the name of the U.S. Government agency and the Government contract number are:

W-7405-ENG-48 (DOE)

Respectfully submitted,

Date 5/28/03

SIGNATURE [signature]

REGISTRATION NO. (if appropriate) 50,938

TYPED or PRINTED NAME Michael C. Staggs

DOCKET IL-10883

TELEPHONE (925) 422-3682

USE ONLY FOR FILING A PROVISIONAL APPLICATION FOR PATENT

60474861 .053003

PATENT

IN THE UNITED STATES PATENT AND TRADEMARK OFFICE

Applicant : The Regents of the University Of California

Attorney Docket No. : IL-10883

Serial No. :

Art Unit:

Filed :

Examiner:

For : Radial Reflection Diffraction Tomography

Commissioner for Patents
Alexandria, VA 22313-1450

EXPRESS MAIL CERTIFICATE

"Express Mail" label number EV268206082US

Date of Deposit May 30, 2003

I hereby certify that the following *attached*

(1) Provisional Application for Patent Cover Sheet (original and one copy)
(2) Provisional Application (Specification 39 pages, drawings included)
(3) Express Mail Certificate
(4) Return postcard

is being deposited with the United States Postal Service "Express Mail Post Office to addressee" service under 37 CFR 1.10 on the date indicated above and is addressed to Mail Stop Provisional Patent Application, Commissioner for Patents, P.O. Box 1450, Alexandria, VA 22313-1450.

April Masluk
(Type or print name of person mailing paper)

April Masluk
(Signature of person mailing paper or fee)

This invention was made in the course of or under prime Contract No. W-7405-ENG-48 between the U.S. Department of Energy and the University of California. This Record of Invention is prepared for the Office of the Assistant General Counsel for Patents, U.S. Department of Energy.

Title of the Invention

Radial Reflection Diffraction Tomography

Inventor(s): those who conceived the invention

LLNL Inventor(s) (First, Middle, Last)

Sean K. Lehman

Abstract of the Invention

This is a new application of diffraction tomography to an annular, outward-looking geometry. An annular array of transducers, or a single or pair of co-located transducers, either electromagnetic or acoustic, directed radially outward, launch a pulse and record the reflected backscattered field. The measured backscattered field is then used in a diffraction tomography reconstruction algorithm to create an image of the material or structure surrounding the transducers.

A diffraction tomographic imaging algorithm has never been developed for this geometry.

The transducers can be located at the end of a catheter which is inserted or "snaked" into an object or part under evaluation.

Uses of the Invention (List past uses, current uses and potential uses for your invention)

LLNL or Government uses or possibilities for use:

- Bore hole tomographic imaging;
- Nondestructive evaluation (NDE) applications such as weapon or material part imaging.

Commercial or other uses or possibilities for use:

- Medical applications such as intravascular ultrasound (IVUS) imaging of blood vessel walls; intestine; prostate.

Background of the Invention

Please describe the background of the invention: what is the technical problem addressed by the invention and what solutions have been used in the past by others (successfully or unsuccessfully).

Intravascular ultrasound (IVUS) imaging provides a method for imaging the interior of blood vessel walls. In standard acoustical imaging techniques, a catheter with a rotating ultrasound transducer is inserted into a blood vessel. The transducer launches a pulse and collects the reflected signals from the surrounding tissue. Current imaging systems use a B-scan mode, whereby images are formed from the envelope of the received signal and by assuming straight ray theory (geometrical optics). These images suffer from the consequences of ray theory of sound propagation which does not model its wave nature.

I propose to develop a new imaging algorithm using diffraction. The technique will still make use of the backscattered field received by current cylindrical IVUS probes. However, because this technique will process both the phase and amplitude of the reflected signal and will properly account for the wave nature of the propagation, it can provide imagery with superior resolution and contrast of both the absorption and sound speed over that provided by existing IVUS systems. The technique is referred to as "radial reflection diffraction tomography" (RRDT) because of the radial configuration of the transducer and the tomographic paradigm used to reconstruct the structure of the tissue from the reflected waves.

The Center for Subsurface Sensing and Imaging Systems (CenSSIS) is a National Science Foundation (NSF) engineering research center headquartered at Northeastern University in Boston, MA. LLNL is a Strategic Affiliate of CenSSIS. Northeastern University, Boston University, and LLNL have applied as CenSSIS members to NSF for funding to develop RRDT into the next generation of

Radial Reflection Diffraction Tomography for Intravascular Imaging

Abstract

Intravascular imaging provides a method for identifying potentially life threatening vulnerable plaque build up on the interior of blood vessel walls. In current acoustical imaging techniques, a catheter with a rotating ultrasound transducer is inserted into a blood vessel. The transducer launches a pulse and collects the reflected signals from the surrounding tissue. Current imaging systems use a B-scan mode, whereby images are formed from the envelope of the received signal and by assuming ray theory (geometrical optics). These images are not able to distinguish between vulnerable and stable plaque. Diagnosis of vulnerable plaque is of clinical importance because its tendency to detach from the vessel wall and cause a stroke.

We propose to develop a new imaging modality, diffraction tomography, to determine plaque structure using intravascular ultrasound (IVUS) probes. The technique will still make use of the back-scattered field received by the cylindrical IVUS probe. However, the technique will provide improved imaging capability because it will make use of both the phase and amplitude of the reflected signal and will properly account for the wave nature of the propagation. The technique is referred to as "radial reflection diffraction tomography" because of the radial configuration of the transducer and the tomographic paradigm is used to reconstruct the structure of the tissue from the reflected waves.

The proposed research will consist of theoretical, numerical and experimental components. The theoretical development of a tomographic algorithm for reflected signals in a radial geometry is an unsolved problem. A novel analytical approach will be developed to obtain a practical inversion scheme. Numerical calculations of the propagation problem will make

use of expertise both at LLNL and BU to simulate ultrasound propagation through an inhomogeneous medium - for both the forward and back-scattered waves. The numerical results will be used to assist in the development of the inversion procedure. The experimental component will be carried out at BU in the CenSSIS MedBED test system. A commercial IVUS probe will be used with either a tissue phantom or in vitro vessel preparation to obtain controlled and repeatable data sets with which to test the inversion algorithm.

The collaboration between LLNL and BU will bring together two groups with complementary expertise to attack the problem of vulnerable plaque. The goal will be to provide a unique approach to characterise the plaque; an approach with a firm theoretical basis that is grounded with results from simulations and experiments. The important societal problem of identifying vulnerable plaque will be advanced by this research.

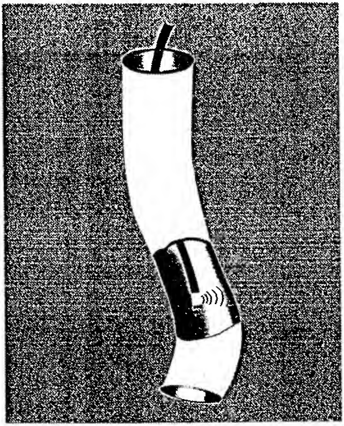

1 Statement of Problem

A rotating wide band transducer, located at the end of a catheter, is snaked into a tube.

The transducer collects reflection mode data at all planar angles at a fixed radius.

The goal is to develop a diffraction tomography imaging technique to reconstruct planar cross-slices of the material surrounding the tube.

Hence the name "radial reflection mode diffraction tomography."

Applications include

- Imaging of blood vessel walls;
- Imaging of specially prepared waste drums with inspection tubes inserted within them;
- The "pig" problem of natural gas and oil pipelines.

The motivation for this is improving current intravascular ultrasound imaging. A catheter is inserted into blood vessels and a rotating ultrasound transducer collects reflection data from the vessel wall. The current imaging technique performs B-scans of the vessel walls. B-scan theory is based upon Beer's law. I wish to extend the imaging technique using diffraction tomography which is based upon the wave equation. I anticipate enhancements in resolution and contrast.

2 Introduction

Operating conditions:

- Transducer rotates at a fixed radius, R_0, about the origin;
- Must use frequency diversity which implies an incident pulse;
- Multimonostatic mode;
- Reflection mode;
- Transducer emits a pulse and records the backscattered field;
- Geometry is that of Figure 2.
  The transducer is located at $\mathbf{r}_0 = R_0\,(\cos\theta, \sin\theta)$.
  The observation point (to be reconstructed) is located at $\mathbf{r}' = r'\,(\cos\theta', \sin\theta')$.
  $R_0 < r'$.

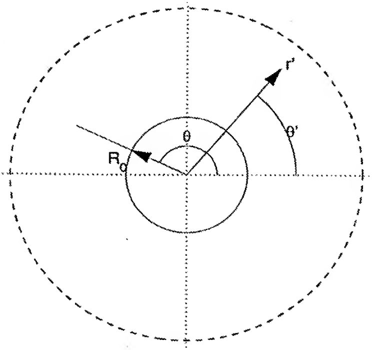
r'
θ'
θ
R0

3 Derivation of Forward Model

Use as fundamental equation the Helmholtz equation,

$$\left[\nabla^2 + k^2(\mathbf{r})\right] u(\mathbf{r},\omega) \;=\; -p(\mathbf{r},\omega), \tag{1}$$

where

$\mathbf{r} \equiv (x,y) = (r,\theta)$	is the spatial coordinate,
ω	is the temporal frequency,
$k(\mathbf{r})$	is the wavenumber of the inhomogeneous medium surrounding the transducer,
$u(\mathbf{r},\omega)$	is the total field,
$p(\mathbf{r},\omega)$	is the incident pulse.

For convenience, drop the explicit ω dependence.

Add $k_0 u(\mathbf{r})$ to both sides of Eqn. 1 where $k_0 \equiv \omega/v_0$, and move the inhomogeneous term to the right hand side:

$$\left[\nabla^2 + k_0^2\right] u(\mathbf{r}) \;=\; -p(\mathbf{r}) - \left[k^2(\mathbf{r}) - k_0^2\right] u(\mathbf{r}). \tag{2}$$

Define the *object function* as

$$o(\mathbf{r}) \;\equiv\; \frac{k^2(\mathbf{r})}{k_0^2} - 1, \tag{3}$$

and express Eqn. 2 as

$$\left[\nabla^2 + k_0^2\right] u(\mathbf{r}) \;=\; -p(\mathbf{r}) - k_0^2 o(\mathbf{r}) u(\mathbf{r}). \tag{4}$$

We may use Green's theorem to cast the differential equation of Eqn. 4 into an integral equation,

$$u(\mathbf{r}) = \int d\mathbf{r}'\, G(\mathbf{r}-\mathbf{r}')\, p(\mathbf{r}') + k_0^2 \int d\mathbf{r}'\, G(\mathbf{r}-\mathbf{r}')\, o(\mathbf{r}')\, u(\mathbf{r}'), \qquad (5)$$

where we have ignored the boundary conditions and

$$G(\mathbf{r}-\mathbf{r}') = \begin{cases} \dfrac{i}{4}\, H_0^{(1)}(k_0\,|\mathbf{r}-\mathbf{r}'|) & n = 2, \\[2ex] \dfrac{1}{4\pi\,|\mathbf{r}-\mathbf{r}'|}\, e^{ik_0|\mathbf{r}-\mathbf{r}'|} & n = 3. \end{cases} \qquad (6)$$

NOTE: Hankel function definition, $H_0^{(1)}(r) \equiv J_0(r) + iN_0(r)$.

The *primary source* is

$$u_i(\mathbf{r}) \equiv \int d\mathbf{r}'\, G(\mathbf{r}-\mathbf{r}')\, p(\mathbf{r}'), \qquad (7)$$

so that Eqn. 5 reads

$$u(\mathbf{r}) = u_i(\mathbf{r}) + k_0^2 \int d\mathbf{r}'\, G(\mathbf{r}-\mathbf{r}')\, o(\mathbf{r}')\, u(\mathbf{r}'). \qquad (8)$$

The *scattered field* is defined as

$$\begin{aligned} u_s(\mathbf{r}) &\equiv u(\mathbf{r}) - u_i(\mathbf{r}), \\ &= k_0^2 \int d\mathbf{r}'\, G(\mathbf{r}-\mathbf{r}')\, o(\mathbf{r}')\, u(\mathbf{r}'). \end{aligned} \qquad (9)$$

Let the measurement surface be at $\mathbf{r}_0 \equiv (R_0, \theta)$ for R_0 fixed and $0 \leq \theta < 2\pi$. Thus, the *measured scattered field* is

$$u_s(\mathbf{r}_0) = k_0^2 \int d\mathbf{r}'\, G(\mathbf{r}_0 - \mathbf{r}')\, o(\mathbf{r}')\, u(\mathbf{r}'). \tag{10}$$

Express $|\mathbf{r}_0 - \mathbf{r}'|$ in polar coordinates:

$$\begin{aligned} |\mathbf{r}_0 - \mathbf{r}'|^2 &= (x_0 - x')^2 + (y_0 - y')^2 \\ &= (R_0 \cos\theta - r' \cos\theta')^2 + (R_0 \sin\theta - r' \sin\theta')^2 \\ &= R_0^2 + r'^2 - 2R_0 r' \cos(\theta - \theta'). \end{aligned} \tag{11}$$

Define

$$\boxed{R^2 \equiv R_0^2 + r'^2 - 2R_0 r' \cos(\theta - \theta').} \tag{12}$$

Thus, in polar coordinates, Eqn. 10 reads

$$\boxed{u_s(R_0, \theta) = k_0^2 \int r' dr' \int d\theta'\, G(R)\, o(r', \theta')\, u(r', \theta').} \tag{13}$$

Eqn. 13 is the forward model of the scattered field. No approximations have been made.

Let the incident field be a point source located at $\mathbf{r}_0$, obeying

$$\left[\nabla^2 + k_0^2\right] u_i(\mathbf{r}' - \mathbf{r}_0) \;=\; -A\,\delta(\mathbf{r}' - \mathbf{r}_0). \tag{14}$$

NOTE: A, the incident pulse amplitude is a function of ω, $A = A(\omega)$.
NOTE: Antenna characteristics are not modeled.

Thus, the incident field is

$$u_i(\mathbf{r}' - \mathbf{r}_0) \;=\; A\,G(R). \tag{15}$$

NOTE: $\mathbf{r}_0 = (R_0, \theta)$ for $0 \le \theta < 2\pi$ is the location of the transceivers; $\mathbf{r}' = (r', \theta')$ for $r' > R_0$ and $0 \le \theta' < 2\pi$ is the location of the observation point. In practice there are N_{trans} discrete transceiver locations. Thus, θ is a discretely index variable, θ_n where $n = 0, 1, \cdots, N_{\text{trans}} - 1$. Thus, Eqn. 13 represents a set of N_{trans} equations.

As is common, invoke the Born approximation,

$$o(\mathbf{r}) \;\equiv\; \frac{k^2(\mathbf{r})}{k_0^2} - 1 \;\approx\; 0, \tag{16}$$

replace the *total field* by the *incident field*, and express Eqn. 13 as

$$\boxed{u_s(R_0, \theta) \approx u_s^B(R_0, \theta) \;\equiv\; A k_0^2 \int r' dr' \int d\theta'\, G^2(R)\, o(r', \theta')} \tag{17}$$

Eqn. 17 serves as our *forward model*.

Now in two- and three-dimensions, we have

$$G(R) \;=\; \begin{cases} \dfrac{i}{4}\, H_0^{(1)}\left(k_0\sqrt{R_0^2 + r'^2 - 2R_0 r' \cos(\theta - \theta')}\right) & n = 2, \\[2ex] \dfrac{e^{ik_0(R_0^2 + r'^2 - 2R_0 r' \cos(\theta - \theta'))}}{4\pi\sqrt{R_0^2 + r'^2 - 2R_0 r' \cos(\theta - \theta')}} & n = 3. \end{cases} \tag{18}$$

NOTE: for $n = 3$, we have assumed all measurements are taken in the same plane so that $z - z' \equiv 0$.

Hankel function expansion from G&R (page 992):

$$\boxed{\begin{aligned} H_0^{(1)}(k_0R) &= \sum_{n=0}^{\infty}(2-\delta_{n0})\ J_n(k_0R_0)H_n^{(1)}(k_0r')\ \cos\left(n(\theta-\theta')\right) \\ &= \sum_{n=-\infty}^{\infty} J_n(k_0R_0)H_n^{(1)}(k_0r')\ e^{in(\theta-\theta')} \end{aligned}} \tag{19}$$

where and $R_0 < r'$.

From M&F page 888, or Morse & Ingard Eqn. 7.3.15:

$$\boxed{\begin{aligned} \frac{e^{ik_0R}}{R} &= i\sum_{n=0}^{\infty}(\delta_{0n}-2)\ \cos(n(\theta-\theta'))\ \times \\ & \int_0^{\infty} kdk\ J_n(kR_0)J_n(kr')\ \frac{e^{i\sqrt{k_0^2-k^2}|z-z'|}}{\sqrt{k_0^2-k^2}}. \end{aligned}} \tag{20}$$

For $z \equiv z'$, we have

$$\boxed{\frac{e^{ik_0R}}{R} = i\sum_{n=0}^{\infty}(\delta_{0n}-2)\ \cos(n(\theta-\theta'))\ \int_0^{\infty} kdk\ \frac{J_n(kR_0)J_n(kr')}{\sqrt{k_0^2-k^2}}} \tag{21}$$

Recall some orthogonality relations...

$$\int_0^{2\pi} d\theta\ \cos(m\theta)\cos(n\theta) = \begin{cases} 2\pi\delta_{mn} & n=0, \\ \pi\delta_{mn} & n\neq 0, \end{cases} \tag{22}$$

$$\int_{-1}^{1} dx\ P_m(x)P_n(x) = \frac{2\delta_{mn}}{2n+1}, \tag{23}$$

or

$$\int_0^{\pi} \sin\theta d\theta\ P_m(\cos\theta)P_n(\cos\theta) = \frac{2\delta_{mn}}{2n+1}. \tag{24}$$

$$\int_0^{2\pi} d\theta\ e^{i(m-n)\theta} = 2\pi\ \delta_{mn} \tag{25}$$

4 Inversion Process Using Two-Dimensional Green's Function

Substitute Eqn. 19 into Eqn. 17:

$$
\begin{aligned}
u_s^B(R_0,\theta) &= -\frac{Ak_0^2}{16}\int r'dr'\int d\theta' \left[\sum_{n=-\infty}^{\infty} J_n(k_0R_0)H_n^{(1)}(k_0r')e^{in(\theta-\theta')}\right]^2 \times \\
&\quad o(r',\theta') \qquad (26) \\
&= -\frac{Ak_0^2}{16}\sum_{m,n=-\infty}^{\infty} J_m(k_0R_0)J_n(k_0R_0)\, e^{i(m+n)\theta} \times \\
&\quad \int r'dr'\int d\theta'\, H_m^{(1)}(k_0r')H_n^{(1)}(k_0r')\, e^{-i(m+n)\theta'}\, o(r',\theta') \qquad (27)
\end{aligned}
$$

Observations regarding Eqn. 27:

- We wish to solve for either the object or the object's spatial spectrum;
- We wish to develop a Fourier Diffraction Theorem for this geometry. This will tell us how the object's spatial spectrum is mapped within this measurement framework;
- We wish to "eliminate" the double summation;
- The spatial integration is less troublesome as this can lead to the Fourier transform of the object function.

Fourier transform Eqn. 27. Define

$$
U_{sm'}^B(R_0) \equiv \int_0^{2\pi} d\theta\, u_s^B(R_0,\theta)\, e^{im'\theta}. \qquad (28)
$$

Multiply both sides of Eqn. 27 by $e^{im'\theta}$ and integrate over θ:

$$
\begin{aligned}
U^B_{sm'}(R_0) &= -\frac{Ak_0^2}{16} \sum_{m,n=-\infty}^{\infty} J_m(k_0R_0)J_n(k_0R_0) \left[\int_0^{2\pi} d\theta\, e^{i(m+n+m')\theta}\right] \times \\
&\quad \int r'dr' \int d\theta'\, H_m^{(1)}(k_0r')H_n^{(1)}(k_0r')\, e^{-i(m+n)\theta'}\, o(r',\theta') \qquad (29)
\end{aligned}
$$

Use

$$
\int_0^{2\pi} d\theta\, e^{i(m-n)\theta} = 2\pi\, \delta_{mn},
$$

so that Eqn. 29 becomes

$$
\begin{aligned}
U^B_{sm'}(R_0) &= -\frac{\pi\, Ak_0^2}{8} \sum_{m,n=-\infty}^{\infty} J_m(k_0R_0)J_n(k_0R_0) \left[\delta_{n,-(m'+m)}\right] \times \\
&\quad \int r'dr' \int d\theta'\, H_m^{(1)}(k_0r')H_n^{(1)}(k_0r')\, e^{-i(m+n)\theta'}\, o(r',\theta') \qquad (30) \\
&= -\frac{\pi\, Ak_0^2}{8} \sum_{m=-\infty}^{\infty} J_m(k_0R_0)J_{-(m'+m)}(k_0R_0) \times \\
&\quad \int r'dr' \int d\theta'\, H_m^{(1)}(k_0r')H_{-(m'+m)}^{(1)}(k_0r')\, e^{im'\theta'}\, o(r',\theta') \qquad (31)
\end{aligned}
$$

Consider the double integral of Eqn. 31:

$$
I = \int r'dr' \int d\theta'\, H_m^{(1)}(k_0r')H_{-(m'+m)}^{(1)}(k_0r')\, e^{im'\theta'}\, o(r',\theta'). \qquad (32)
$$

Replace $o(r',\theta')$ by its Fourier transform:

$$
\begin{aligned}
o(r',\theta') &= \frac{1}{2\pi} \int dk_x \int dk_y\, O(k_x,k_y)\, e^{-i(k_xx'+k_yy')} \qquad (33) \\
&= \frac{1}{2\pi} \int dk_x \int dk_y\, O(k_x,k_y)\, e^{-ir'(k_x\cos\theta'+k_y\sin\theta')}. \qquad (34)
\end{aligned}
$$

Then Eqn. 32 reads,

$$
\begin{aligned}
I &= \frac{1}{2\pi} \int dk_x \int dk_y\, O(k_x,k_y) \times \\
&\quad \int r'dr' \int d\theta'\, H_m^{(1)}(k_0r')H_{-(m'+m)}^{(1)}(k_0r') \times \\
&\quad e^{im'\theta'}\, e^{-ir'(k_x\cos\theta'+k_y\sin\theta')}, \qquad (35) \\
&= \frac{1}{2\pi} \int dk_x \int dk_y\, O(k_x,k_y) \times \\
&\quad \int r'dr'\, H_m^{(1)}(k_0r')H_{-(m'+m)}^{(1)}(k_0r') \times \\
&\quad \int d\theta'\, e^{im'\theta'}\, e^{-ir'(k_x\cos\theta'+k_y\sin\theta')}, \qquad (36)
\end{aligned}
$$

4.1 Method 1 for Inversion

Summarizing, we have

$$
\begin{aligned}
U^{B}_{sm'}(R_0) &= -\frac{\pi A k_0^2}{8} \sum_{m=-\infty}^{\infty} J_m(k_0R_0)J_{-(m'+m)}(k_0R_0) \times \\
&\quad \int r'dr' \int d\theta' \, H_m^{(1)}(k_0r')H^{(1)}_{-(m'+m)}(k_0r') \, e^{im'\theta'} \, o(r',\theta') \qquad (37) \\
&= -\frac{\pi A k_0^2}{8} \int r'dr' \int d\theta' \, o(r',\theta') \, \times \\
&\underbrace{\sum_{m=-\infty}^{\infty} J_m(k_0R_0)J_{-(m'+m)}(k_0R_0) \, H_m^{(1)}(k_0r')H^{(1)}_{-(m'+m)}(k_0r') \, e^{im'\theta'}}_{\text{Need a summation formula}} \qquad (38)
\end{aligned}
$$

4.2 Method 2 for Inversion

Summarizing, we have

$$
\begin{aligned}
U^{B}_{sm'}(R_0) &= -\frac{\pi A k_0^2}{8} \sum_{m=-\infty}^{\infty} J_m(k_0R_0)J_{-(m'+m)}(k_0R_0) \times \\
&\quad \int r'dr' \int d\theta' \, H_m^{(1)}(k_0r')H^{(1)}_{-(m'+m)}(k_0r') \, e^{im'\theta'} \, o(r',\theta'). \qquad (39)
\end{aligned}
$$

Define

$$
\begin{aligned}
V_{mm'} &= \int r'dr' \int d\theta' \, H_m^{(1)}(k_0r')H^{(1)}_{-(m'+m)}(k_0r') \, e^{im'\theta'} \, o(r',\theta') \\
&= \int r'dr' \, H_m^{(1)}(k_0r')H^{(1)}_{-(m'+m)}(k_0r') \underbrace{\int d\theta' \, o(r',\theta') \, e^{im'\theta'}}_{\equiv O_{m'}(r')} \\
&= \underbrace{\int r'dr' \, H_m^{(1)}(k_0r')H^{(1)}_{-(m'+m)}(k_0r') \, O_{m'}(r')}_{\text{Use orthogonality relation}} \qquad (40)
\end{aligned}
$$

So Eqn. 39 reads

$$
U^{B}_{sm'}(R_0) = -\frac{\pi A k_0^2}{8} \sum_{m=-\infty}^{\infty} J_m(k_0R_0)J_{-(m'+m)}(k_0R_0) \, V_{mm'} \qquad (41)
$$

Solve Eqn. 41 for $V_{mm'}$ in terms of the known measured scattered field transform, $U^{B}_{sm'}(R_0)$. Then solve Eqn. 40 for $O_{m'}(r')$ in terms of $V_{mm'}$.

Radial Reflection Diffraction Tomography

1 Problem Definition

We propose to develop a new nondestructive evaluation (NDE) modality using diffraction tomography (DT) to image the internal structures of media in cases where it is infeasible to use external NDE systems. We assume the object under evaluation has existing holes or access ports to its interior. We envision a probe-bearing catheter or tube being inserted or "snaked" into the structure. The probe consists of a rotating, outward-looking, transducer, or alternatively, an annular array of outward-looking transducers. At each angular location, the transducer(s) launch a pulse[1] and collect the reflected (backscattered) field.

Since the transducer rotates at a fixed radius about the center of the catheter collecting reflected field information, and since we will use DT techniques to process the data, we refer to this technique as "Radial Reflection Diffraction Tomography" (RRDT). Diffraction tomography has never been applied to this geometry.

We are seeking support over three years to develop the basic RRDT algorithm the first year and to investigate differing data collection modalities (multimonostatic, multibistatic, etc.), a full wave algorithm the second, and prototype hardware during the third. Applications include bore hole tomographic imaging, NDE inspection of the internal structures of objects, and the medical areas of intravascular ultrasound (IVUS) and prostate imaging.

This project is part of a collaboration between Lawrence Livermore National Laboratory; the institutions of Boston University (BU) and Northeastern University (NU) through the auspices of the Center for Subsurface Sensing and Imaging Systems (CenSSIS), a National Science Foundation Engineering Research Center (LLNL is a Strategic Affiliate of CenSSIS); the Center for Integration of Medicine and Innovative Technology (CIMIT) within Massachusetts General Hospital (MGH); and the medical equipment manufacturers of Boston Scientific and Analogic. The interests of the other participants is to develop the next generation IVUS device.

Intravascular ultrasound imaging provides a method for identifying potentially life threatening vulnerable plaque build up on the interior of blood vessel walls. In standard acoustical imaging techniques, a catheter bearing a rotating ultrasound transducer or cylindrical ultrasound array, is inserted into a blood vessel. The transducer launches a pulse and collects the reflected signals from the surrounding tissue. Current imaging systems use a B-scan mode, whereby images are formed from the envelope of the received signal and by assuming straight ray theory (geometrical optics). These images suffer from the consequences of ray theory of sound propagation which does not model its wave nature.

The RRDT theory development is general and is applicable to any NDE problem in which it is infeasible to image a structure using existing exterior scanning systems. Thus, the RRDT algorithm developed for bore hole or NDE applications can be used on the medical project.

2 Problem Importance

An outward-looking radial reflection diffraction tomography system has never been developed. Yet many situations exist where such a system would be a valuable tool for non-invasive imaging.

Consider the bore hole tomography case show in Figure 1. An RRDT probe can lowered into the bore hole to image the site and to determine the state and location of buried wastes, and to track plumes of underground contaminants. In a similar manner, probes can be inserted into waste drum barrels, or weapons to image and determine the state of the material.

[1] Either acoustic or electromagnetic.

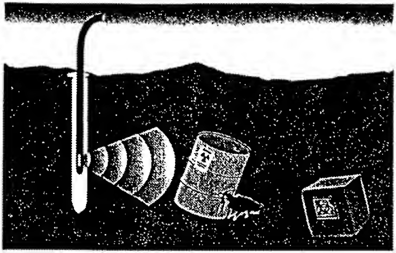

Figure 1: *Application of RRDT bore hole tomography which demonstrates the similar radial reflection geometry as IVUS.*

The IVUS geometry is identical to that of the NDE applications in that a catheter inserted into a blood vessel is similar to that of a cylindrical probe in an bore hole or mechanical part. The RRDT algorithms and technology developed for NDE will transport easily across to the problem of IVUS diffraction tomography.

The medical application is significant in that atherosclerosis, a condition where the arteries are obstructed by the build up of deposits, "intravascular plaque" (IVP), on the inside of arterial walls, is the third leading cause of death and the leading cause of major disability amongst adults. Of particular concern is plaque that is vulnerable (or unstable), as two-thirds of the 1.1 million heart attacks that occur annually in the United States occur when these vulnerable plaques become inflamed, and then suddenly and unexpectedly rupture. There is no accepted modality for the classification of artherosclerotic plaque to determine whether it is vulnerable or not. This is a barrier to successful diagnosis and subsequent treatment.

Plaque is broadly divided into two types [1, 2]. Stable or non-vulnerable plaque, typically consisting of a thick layer of fibrous tissue, is not life threatening and can be treated slowly. Vulnerable plaque is typically characterized by a thin fibrous cap covering a pool of soft lipid core. When the vulnerable plaque is disrupted, the thin cap is compromised and the lipid deposited into the artery can produce adverse effects, such as thrombus formation, strokes, and death. If vulnerable plaque can be identified early, it could be treated medically to reduce the risk of rupture.

3 Directorate Alignment

This work aligns with the Center for Nondestructive Characterization (CNDC) and advances the core competencies of advanced sensors and instrumentation, as well as biotechnology and health care.

4 Problem Payoff

The problem payoff is in the development of the theory behind a new and versatile method of diffraction tomographic imaging with applications in NDE and medicine. Additionally, the collaboration with the universities provides LLNL with access to a source of to undergraduate, graduate and post-doctoral students. Through CenSSIS, the medical equipment manufacturers of Boston Scientific and Analogic are prepared to construct an RRDT IVUS system.

5 Approach

This work directly aligns with CNDC. The goal of the first year is to develop a general RRDT theory and inversion algorithm, and then specialize it to the IVUS problem.

The development of the RRDT IVUS algorithm will be the Laboratory's contribution to the collaboration between the other CenSSIS participants, MGH, Boston Scientific, and Analogic. The RRDT component includes the development of the forward scattering model, the development of the inversion theory and algorithm, FDTD simulation of the various applications which will be performed using Laboratory developed finite-difference time-domain (FDTD) codes, reconstruction of the simulated data, and verification of the inversion algorithm.

We are seeking LDRD funding to support the RRDT algorithm development aspect of the larger RRDT IVUS effort. The other research partners will be funded either directly through CenSSIS or through their respective institutions.

The larger research plan including the collaborators consists of three parallel tracks with the common goal of RRDT IVUS algorithm validation and tissue classification. The tracks are *Numerical Studies*, *Scale Model Phantoms*, and *In Vitro Tissue Experiments* as indicated in the flow chart of Figure 2. The track descriptions are the following:

- *In vitro* tissue pathology samples will be analyzed at BU using a scanning acoustic microscope (SAM) to determine their sound speed and absorption properties. Histological analysis performed at MGH will identify the tissue types. By combining these results, we will develop a mapping from observed acoustic properties to tissue types. This will permit us to classify tissues based upon observed acoustic results. The tissue characterization will be used to develop the numerical and tissue mimic phantoms used in the numerical simulations and laboratory scaled IVUS tracks, respectively. Once RRDT has been implemented, experiments performed at BU on *in vitro* tissue samples using a Boston Scientific IVUS system will be used to collect radial reflection mode data to be used in the RRDT IVUS inversion algorithm.

- **Numerical.** LLNL developed FDTD codes will be used to perform numerical simulations. They will model full acoustic wave propagation under tightly controlled (numerical) experiments, and are flexible enough to model both the bore hole and vascular media. They will generate numerical radial reflection mode data to be used in the RRDT inversion algorithm.

- **Phantoms.** Scale model tissue mimic phantoms will be developed at BU using the results of the tissue characterization. They will be used in controlled, scaled IVUS experiments to generate experimental radial reflection mode data to be used in the RRDT IVUS inversion algorithm.

The results of each of these tracks are reconstructed images of medium (bore hole, tissue, or other object of interest) sound speed and absorption. The quality of the images will be validated using the numerical phantoms, experimental phantoms, and *in vitro* tissue samples. The images will be characterized and their components identified. For example, the tissue types will be classified as stable plaque, vulnerable plaque, lipid pool, etc., using the tissue characterization results.

Common to all of the tracks is the development of an efficient, robust inversion scheme for RRDT. The forward RRDT model will be validated and analyzed for accuracy using the knowledge gained from the numerical and experimental components.

5.1 Details of the Radial Reflection Diffraction Tomography Inversion Algorithm

In RRDT, a single transducer rotates at a fixed radius about the center of the probe. At each angular location, the transducer launches a pulse into the medium and collects the returned backscattered field. This is known as a multimonostatic operating mode.[2] Current IVUS imaging techniques rely upon a straight-ray model of sound propagation [3, 4]. That is, the sound waves travel in straight lines subject only to reflection, material absorption, and geometrical spreading due to distance traveled.[3] Variants of the model may or may not take into account refraction, that is, the bending of rays at interfaces, and none account for the wave nature of diffraction. The reconstructed images, formed from the magnitude of the backscattered returns, show only attenuation[4] maps of the medium.

[2] An alternative design would be an array of fixed transducers located on an annulus. This would constitute either a bistatic or multibistatic operating mode, depending upon the configuration.

[3] This is also known as "$1/r$" attenuation.

[4] That is, amplitude loss due to the combined effects of absorption, reflection, and refraction.

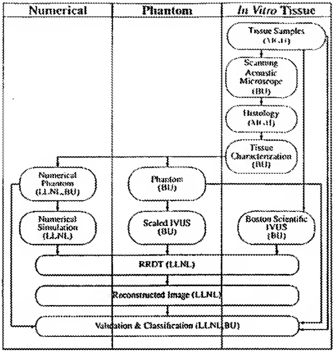

Figure 2: *RRDT IVUS project development flow chart. The LLNL contributions to the project are as indicated.*

During the first year, we propose using a wave-based diffraction tomography (DT) model which more accurately models the wave nature of the sound propagation. Since DT algorithms make use of both the magnitude and phase of the backscattered returns, the reconstructions are complex quantities representing the sound speed and absorption of the medium. During the second year, we will implement a full wave algorithm which is quantitatively more accurate than the DT algorithm which is based upon the Born approximation. The third year will be used to develop practical hardware for LLNL usage.

Although DT has been applied to various NDE and medical imaging problems, the technique has never been applied to the outwardly directed radial geometry operating in a reflection mode. A DT inversion algorithm for this geometry, that is, a radial reflection diffraction tomography, algorithm has never been developed. The outline of the forward RRDT model derivation and a discussion of its inversion is presented in Appendix A.

5.2 Reconstructed Images and Validation

The images reconstructed by the RRDT algorithm will be compared to the actual input acoustic data and their corresponding histological maps for validation and classification. We will first evaluate the performance of RRDT when used to invert signals from numerical models and scaled experimental models. The performance of RRDT can then be evaluated in a controlled environment. At this stage, different monostatic and bistatic transducer geometries can be evaluated in order to determine the best and most practical option to implement.

6 PI and Team

Sean K. Lehman, Ph.D., is an LLNL engineer with experience in remote sensing, straight ray tomography, and diffraction tomography. He will be developing the RRDT theory and inversion algorithm, and FDTD modeling.

LLNL engineer with experience in wave theory, inverse problems, diffraction and full wave tomography. He will be consulting on the RRDT theory and inversion algorithm.

8 Reporting Schedule

The reporting schedule for the RRDT theory and inverse algorithm development is

1. Develop the forward model;
2. Develop the RRDT inverse algorithm;
3. Perform FDTD simulation;
4. Perform RRDT inverse on FDTD simulation results. Perform RRDT inverse on experimental results from BU;
5. Validate RRDT inverse algorithm.

The time line for the overall RRDT IVUS project is shown in Figure 3

9 Deliverables

The deliverables are

1. The forward RRDT model, inversion algorithm, and computer codes;
2. Peer reviewed published papers;
3. The acoustical properties of blood vessel tissue components.

10 Exit Plan

With the successful development of an RRDT imaging algorithm, we will seek funding to develop an NDE tool. Additionally, we anticipate licensing the RRDT IVUS software to the medical equipment manufacturers for use in the next generation IVUS systems.

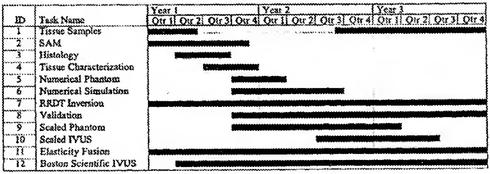

Figure 3: *RRDT IVUS project time line.*

A Derivation of Forward RRDT Model

The goal of any DT algorithm is to invert the forward wave-based model. Our wave equation model is an accurate description of sound propagation valid for a fluid with arbitrary inhomogeneities and thermoviscous absorption [5].

$$\nabla^2 p(\mathbf{r},t) - \frac{1}{c^2(\mathbf{r})}\partial_t^2 p(\mathbf{r},t) + \frac{\delta_{TV}(\mathbf{r})}{\rho(\mathbf{r})c^4(\mathbf{r})}\partial_t^3 p(\mathbf{r},t) - \frac{\nabla\rho(\mathbf{r})}{\rho(\mathbf{r})}\cdot\nabla p(\mathbf{r},t) = -q(\mathbf{r},t). \tag{1}$$

Here $p(\mathbf{r},t)$ is the acoustic pressure, $q(\mathbf{r},t)$ the source, $\rho(\mathbf{r})$ the density of the medium, $c(\mathbf{r})$ is the sound speed of the medium and $\delta_{TV}(\mathbf{r})$ is the acoustic diffusivity. The diffusivity accounts for both thermal and viscous losses in the fluid, and is related to the acoustic absorption coefficient, $\alpha(\mathbf{r})$, via

$$\delta_{TV}(\mathbf{r}) = 2\,\frac{\alpha(\mathbf{r})c^3(\mathbf{r})}{\omega^2}, \tag{2}$$

where ω is the temporal angular frequency.

There are problems, however, in inverting the full wave equation of Eqn. 1 for the two unknown parameters of sound speed, $c(\mathbf{r})$, and absorption, $\alpha(\mathbf{r})$, because the density, $\rho(\mathbf{r})$, appears as a spatially varying quantity. We must simplify the full forward model of Eqn. 1. The simplification arises from the fact the tissue density does not vary significantly. That is, there is negligible density variation across tissue types. With this simplification, the $\nabla\rho(\mathbf{r})$ is identically zero and Eqn. 1 reduces to

$$\left[\nabla^2 - \frac{1}{c^2(\mathbf{r})}\partial_t^2 + \frac{\delta_{TV}(\mathbf{r})}{\rho_0 c^4(\mathbf{r})}\partial_t^3\right] p(\mathbf{r},t) = -q(\mathbf{r},t), \tag{3}$$

where we have replaced $\rho(\mathbf{r})$ with a uniform background density ρ_0.

Fourier transforming Eqn. 3 in time, we achieve the Helmholtz equation,

$$\left[\nabla^2 + k^2(\mathbf{r})\right] p(\mathbf{r},\omega) = -q(\mathbf{r},\omega), \tag{4}$$

where ω is the temporal frequency, and the complex wavenumber distribution is defined in terms of the absorption,

$$k^2(\mathbf{r}) = \frac{\omega^2}{c^2(\mathbf{r})} - i\,\frac{2\alpha(\mathbf{r})\omega}{\rho_0 c(\mathbf{r})}, \tag{5}$$

where, in tissue, the absorption increases linearly with frequency, that is, $\alpha(\mathbf{r}) \approx \alpha_0(\mathbf{r})\omega$. It is convenient to express Eqn. 4 in a form in which the inhomogeneity appears on the right hand side. We do so by adding $k_0^2(\omega)p(\mathbf{r},\omega)$ to sides of the equation and moving the $k^2(\mathbf{r})p(\mathbf{r},\omega)$ inhomogeneity to the right hand side:

$$\left[\nabla^2 + k_0^2(\omega)\right] p(\mathbf{r},\omega) = -q(\mathbf{r},\omega) - k_0^2(\omega)\, o(\mathbf{r})\, p(\mathbf{r},\omega). \tag{6}$$

where the *background* wavenumber is $k_0(\omega) \equiv \omega/c_0$ and the *object distribution function* is $o(\mathbf{r}) \equiv k^2(\mathbf{r})/k_0^2(\omega) - 1$. We note that we have expressed the object distribution as being independent of frequency, that is, dispersionless. We show this by substituting Eqn. 5 into the definition of the object distribution function. After simplification, we find

$$o(\mathbf{r}) = n^2(\mathbf{r}) - 1 - i\,\frac{2\alpha_0(\mathbf{r})n(\mathbf{r})c_0}{\rho_0}, \tag{7}$$

where $n(\mathbf{r}) \equiv c_0/c(\mathbf{r})$ is the *index of refraction*. Thus, as long as medium's sound speed and density are independent of frequency[5], so is the object distribution. This is not only a valid assumption [6], but essential to the final inversion algorithm as explained below. In practice, the reconstructed sound speed and absorption distributions represent values averaged over the insonifying frequency bandwidth.

Eqn. 6 is no easier to solve than Eqn. 4, however it "appears" easier in that the left hand side contains no spatial inhomogeneities. The right hand side appears to have two source terms: a *primary* source term, $q(\mathbf{r},\omega)$; and a *secondary* source term given by $k_0^2(\omega)o(\mathbf{r})p(\mathbf{r},\omega)$.

[5] or slowly varying with frequency

Using Green's Theorem [7, 8], we convert Eqn. 6 from a differential to an integral equation:

$$p(\mathbf{r},\omega) \;=\; \int d\mathbf{r}'\, G(\mathbf{r}-\mathbf{r}',\omega)\, q(\mathbf{r}',\omega) + k_0^2(\omega) \int d\mathbf{r}'\, G(\mathbf{r}-\mathbf{r}',\omega)\, o(\mathbf{r}')\, p(\mathbf{r}',\omega), \tag{8}$$

where $G(\mathbf{r},\omega)$ is the free space Green's function,

$$G(\mathbf{r}-\mathbf{r}',\omega) \;=\; \frac{e^{ik_0(\omega)|\mathbf{r}-\mathbf{r}'|}}{4\pi|\mathbf{r}-\mathbf{r}'|}.$$

We observe that the total field is the sum of two components. The first term on the right hand side is defined as the *incident* or insonifying field, $p_i(\mathbf{r},\omega)$. The *scattered* field is thus

$$p_s(\mathbf{r},\omega) \;=\; k_0^2(\omega) \int d\mathbf{r}'\, G(\mathbf{r}-\mathbf{r}',\omega)\, o(\mathbf{r}')\, p(\mathbf{r}',\omega). \tag{9}$$

When we evaluate Eqn. 9 at a set of receivers or receiver locations, we obtain an integral relationship between the known measured scattered field, $p(\mathbf{r},\omega)$, and the unknown object distribution, $o(\mathbf{r})$.

Eqn. 9, however, is very difficult to solve as the scattered field, $p_s(\mathbf{r},\omega)$ appears on both sides of the equation, entering implicitly as part of the total field, $p(\mathbf{r},\omega)$. We simplify the problem by taking advantage of the physical fact the acoustic properties of the insonified tissue vary little from the background (assumed to be water). Mathematically, we express this as $k(\mathbf{r}) \approx k_0(\omega)$.

The implication is that we may neglect the scattered field term within the integral and replace the total field by the incident field. This is known as the ***Born approximation***. We then express the scattered field as

$$p_s(\mathbf{r},\omega) \approx p_s^B(\mathbf{r},\omega) \;=\; k_0^2(\omega) \int d\mathbf{r}'\, G(\mathbf{r}-\mathbf{r}',\omega)\, o(\mathbf{r}')\, p_i(\mathbf{r}',\omega), \tag{10}$$

where the B superscript indicates we are operating under the Born approximation.

We now consider the geometry of an IVUS scan shown in Figure 4 (b) and specialize Eqn. 10 to the case of a single rotating transducer which launches a pulse and collects the backscattered data at discrete angular locations. The transducer is located at the fixed radius of R_0. Its angle of rotation is θ. Vectorially, we indicate the transducer location and observer points as $\mathbf{r}_0 = R_0\ (\cos\theta, \sin\theta)$ and $\mathbf{r}' = r'\ (\cos\theta', \sin\theta')$, respectively. With this notation, Eqn. 10 reads

$$\boxed{p_s^B(\mathbf{r}_0,\omega) \;=\; k_0^2(\omega) \int_{R_0}^{\infty} r' dr' \int_0^{2\pi} d\theta'\, G(\mathbf{r}_0-\mathbf{r}',\omega)\, o(\mathbf{r}')\, p_i(\mathbf{r}',\omega).} \tag{11}$$

Eqn. 11 is our forward IVUS imaging model. It represents a mathematical mapping of the object distribution from the (r',θ') object space to the (θ,ω) measurement space. In operator notation, we express this as

$$p_s^B(\theta,\omega) \;=\; \mathcal{K}(\theta,\omega;r',\theta')\, o(r',\theta'), \tag{12}$$

where the *forward scattering operator*, $\mathcal{K}(\theta,\omega;r',\theta')$ is defined as

$$\mathcal{K}(\theta,\omega;r',\theta')[\,\cdot\,] \;\equiv\; k_0^2(\omega) \int_{R_0}^{\infty} r' dr' \int_0^{2\pi} d\theta'\, G(\mathbf{r}_0-\mathbf{r}',\omega)\, p_i(\mathbf{r}',\omega)\, [\,\cdot\,]. \tag{13}$$

Eqn. 11, or equivalently Eqn. 12, is the equation we propose to invert for RRDT imaging whether IVUS or bore hole related; whether monostatic or bistatic. $p_s^B(\theta,\omega)$ is the known measured scattered field at the transducer at angular location θ and frequency ω. Thus, in operator notation, we may solve Eqn. 12 for the unknown object distribution via

$$o(r',\theta') \;=\; \mathcal{K}^{-1}(\theta,\omega;r',\theta')\, p_s^B(\theta,\omega). \tag{14}$$

The inversion algorithm will determine an expression for $\mathcal{K}^{-1}(\theta,\omega;r',\theta')$, a mapping from the (θ,ω) measurement space back to the (r',θ') object space. This inverse mapping operator will involve integration over temporal frequency variable, ω, and the angular observation variable, θ, to recover the two object spatial variables (r',θ'). It will recover

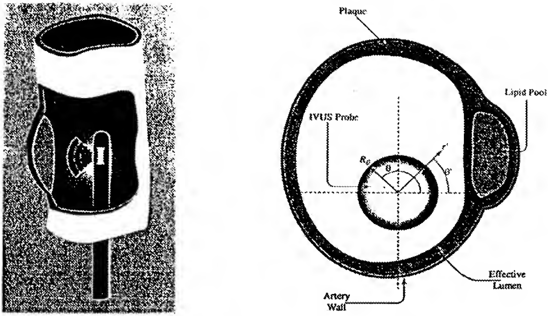

(a) (b)

Figure 4: *IVUS artery scan schematic and cross-slice geometry. (a) A catheter with a probe inserted into an artery scans a region around a plaque build up. (b) Cross-slice detail of the IVUS scan showing the vessel structure and variables used in the RRDT scan geometry.*

the two-dimensional complex object distribution, $o(\mathbf{r}')$, from which we can obtain the sound speed and absorption through Eqn. 5.

Considering the operator notation of Eqn. 12, it becomes clear why the object distribution must be dispersionless. Our goal is to reconstruct a two-dimensional object. The forward operators maps the object from a two-dimensional space to another two-dimensional space. Thus, we have a sufficient number of free, independent variables to derive an inverse mapping [9]. If the object distribution were a function of frequency as well, the forward mapping would represent a type of projection operator from the three-dimensional (r', θ', ω) space to the two-dimensional (r, ω) space and we would have an insufficient number of free variables to develop and perform the inverse mapping.

In developing the inversion algorithm, we will invert the model for two differing operating modes: monostatic and bistatic. In the former case, the transmitting and receiving transducer are co-located, while in the latter, they are separate and independent. We believe an analytic inverse is possible in both operating modes. Should this not be the case, we intend to develop a numerical inverse based upon a moment method expansion of the object distribution.

Radial Reflection Diffraction Tomography for Intravascular Imaging with Application to Classifying Atherosclerotic Plaque

1 Overview

This Partnerships in Education and Research (PER) proposal is focused upon enhancing the collaboration of our ERC with industry, a national laboratory, and a major federally funded center of excellence. The project is focused upon the development of a new approach to sensing and imaging the presence of structures within cardiac arteries that are believed to be correlated with the triggering of sudden, unexpected heart attacks. The PER funding would enable the Center for Subsurface Sensing and Imaging Systems (CenSSIS) to assemble the multi-disciplinary team and the resources needed to address the important societal problem. Our approach will be to create a next generation instrument using the technique of Intravascular Ultrasound (IVUS).

The CenSSIS long-range mission is to revolutionize mankind's ability to probe into hidden worlds. An overarching theme is the development of a new discipline for subsurface sensing and imaging (SSI) through the development of a unified discipline that encompasses diverse applications. The impact of CenSSIS is that "diverse problems have similar solutions." Detection of the structures that trigger heart attacks is a potent example of the philosophy. By developing a modality to solve the IVUS problem we believe we will also be able to address the issue borehole classification of buried waste – a problem of interest to the environmental engineering community.

CenSSIS is a new ERC, still within its first year of operation. In the next few years the Center must create the enabling testbed infrastructure that will lead it toward the engineered system I-PLUS (Integrated Probes to Look Under Surfaces). In the CenSSIS strategic plan we identify the need to attack real problems as an endeavor to begin in Year 3. There is an impetus from industry and our federally funded collaborators to accelerate that strategic timetable. This PER proposal is a response to that impetus.

In addition to the PER funding requested from NSF we have marshaled significant cost sharing resources from industry and our other federally funded organizations. These resources are detailed in our budget section but amount to over $400,000 over the three year project period. In terms of industry collaboration, Boston Scientific, Inc. and Analogic, Inc. will become new members of CenSSIS partially contingent upon the ability of CenSSIS to undertake the IVUS effort.

A strategic goal for CenSSIS is the involvement of medical imaging and instrumentation manufactures such as the two major corporations in the PER collaborative. The definition of the IVUS initiative was a critical factor in sparking the interest of a corporate sector that is traditionally focused upon short term delivery of new products to a hotly competitive marketplace. Since the IVUS project is an unrestricted basic research initiative it will serve as a magnet to attract other medical sector companies into the CenSSIS fold.

Lawrence Livermore National Laboratory (LLNL) has a traditional mission to develop new technologies for the environmental and non-destructive evaluation sectors. The laboratory is strategically targeting the medical imaging sector as one to enhance the portfolio of the prestigious organization. Additionally, the interest of LLNL in the bore-hole waste and contaminant imaging problem which is mathematically related to the plaque imaging problem, falls within the realm of the SoilBED of CenSSIS. We anticipate that data from this project would provide ideal pilot data for SoilBED to implement this imaging modality. Because of this project's importance and relevance, LLNL has provided all of Dr. Lehman's funding on this effort.

Finally The Center for Integration of Medicine and Innovative Technology (CIMIT) within Massachusetts General Hospital (MGH) has identified the detection of heart attack triggering factors as one of their major targets. Hence

CIMIT is willing to invest "New Concept" funds to augment this PER effort. Both LLNL and MGH are already strategic affiliates of CenSSIS. The PER cost share is an augmentation of their collaboration.

2 Introduction

Atherosclerosis is a condition where the arteries are obstructed by the build up of deposits, "intravascular plaque" (IVP), on the inside of arterial walls. Atherosclerotic cerebrovascular disease is the third leading cause of death and the leading cause of major disability amongst adults. Of particular concern is plaque that is vulnerable (or unstable), as two-thirds of the 1.1 million heart attacks that occur annually in the United States occur when these vulnerable plaques become inflamed, and then suddenly and unexpectedly rupture. There is no accepted modality for the classification of artherosclerotic plaque to determine whether it is vulnerable or not. This is a barrier to successful diagnosis and subsequent treatment.

Plaque grows as a fibrous tissue encapsulating lipid pool. As the plaque grows it may incorporate calcium. Plaque is broadly divided into two types [1, 2]. Stable or non-vulnerable plaque, typically consisting of a thick layer of fibrous tissue, is not life threatening and can be treated slowly. Vulnerable plaque is typically characterized by a thin fibrous cap covering a pool of soft lipid core. Figure 1 shows arterial cross-slice examples of each type of plaque. When the plaque is disrupted, the thin cap is compromised and the lipid deposited into the artery can produce adverse effects, such as thrombus formation, strokes, and death. If vulnerable plaque can be identified it could be treated aggressively to reduce the risk of rupture. Surgical treatment includes implanting a stent, or wire mesh, inside the blood vessel to hold back any obstruction. In addition, cholesterol-lowering medications have been shown to lessen a chance of a rupture by somehow stabilizing the plaques.

Many modalities exist currently that can detect the presence of plaque in arteries. These include: treadmill stress tests, which monitor patients' hearts while they exert themselves; cardiac catheterization for intravascular ultrasound (IVUS), elasticity imaging, and optical coherence tomography (OCT); external ultrasound; Raman spectroscopy; angiograms; MRI [3]; and electron beam computed tomography (EBCT) which detects calcifications not plaque. These techniques are capable of estimating plaque burden. None of the methods provide sufficient accuracy for their results to be used by doctors to order the drastic surgery that is often associated with the diagnosis.

We propose to use traditional IVUS probes, both single element and cylindrical arrays, to obtain ultrasound data from vessels. We will process the received signals using a novel technique *radial reflection diffraction tomography* (RRDT) to extract additional characteristics of the tissue above and beyond traditional B-scan imaging. Further, we plan to implement *information fusion* by combining RRDT images with images generated by quantitative elasticity imaging. The elasticity images will provide information about the stiffness of the material that will be complementary to the acoustic parameters recovered by RRDT. We anticipate that the techniques will remove the classification barrier to facilitate the identification of vulnerable plaque.

3 Background

A typical IVUS method of operation is presented in Figure 2 (a). A catheter bearing a cylindrical IVUS probe is inserted into a diseased artery. The artery is nominally circular, with a non-centered probe. Around the wall of the artery is the fibrous collagen plaque. Inside this fibrous structure is a lipid pool as shown in Figure 2 (a) and indicated in the cross-slice graphic of Figure 2 (b). When the fibrous cap separating the lipid pool from the blood in the artery is more than 800 μm thick, the plaque is considered stable. However, in cases where the cap is less than about 300 μm thick, the plaque is considered vulnerable, and is much more likely to rupture.

Current IVUS probes collect data using a standard pulse-echo technique. An acoustic beam is transmitted into the tissue and a single B-scan line is formed from the received signal in the same direction. A circumferential scan is made by either rotating a single transducer (mechanical beam steering) or by phasing an array of transducers around the circumference (electronic beam forming). A representative image of the former technique is presented in Figure 3. The later technique is more complicated but allows more control of the signals generation and gives greater ability to improve the signal capture [4].

Although B-scan IVUS images are successful at detecting plaque and being able to characterize its volume [5], the classification of plaque types by ultrasound is very difficult. Conventional B-scan images are formed from scattering which, in turn, depends on the acoustic impedance dissimilarity of tissue types and structures. Although relatively

(a) (b)

Figure 1: *Artery cross-slices. (a) Non-vulnerable plaque with fibrous tissue that partially blocks blood flow but not likely to cause a clot or cardiac event. (b) Vulnerable plaque with a lipid rich core and a thin fibrous cap. Images courtesy of CIMIT and Drs. Kraman Purushothamen and William O'Conner.*

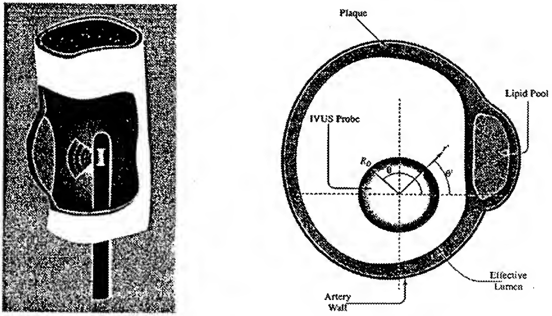

(a) (b)

Figure 2: *IVUS artery scan schematic and cross-slice geometry. (a) A catheter with a probe inserted into an artery scans a region around a plaque build up. (b) Cross-slice detail of the IVUS scan showing the vessel structure and variables used in the RRDT scan geometry.*

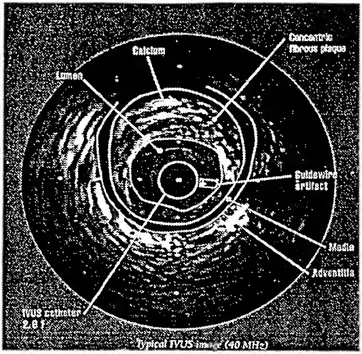

Figure 3: *In vivo IVUS image taken with a single 40 MHz transducer. Photograph courtesy of Boston Scientific.*

hard calcifications in some plaque can be detected using this mismatch [6], the similarity in the acoustic properties of fibrous plaque and lipid pools prevents direct identification. Consequently, the size of the fibrous cap cannot be accurately estimated [7].

Diffraction tomography has been applied to medical imaging problems for a number of years [8, 9], usually in a standard circumferential through transmission mode. Time domain diffraction tomographic images [9] have shown increased clarity, resolution and contrast because of the correct accounting of wave propagation and the use of redundant information in multiple angular views of the objects imaged. A related B-mode approach, spatial compounding, also provides improved vascular images through multiple look angles [10].

The diffraction tomography approach we propose is an outwardly directed radial geometry which employs reflection rather than transmission. This geometry is suited to IVUS probes. In Figure 4, typical angularly incremented beams from a single rotating IVUS transducer show significant overlap. This valuable overlap information is lost in normal B-mode processing. Through the use of our unique RRDT processing, which accounts for phase and amplitude and beam diffraction, this information can be recovered to provide images with improved lateral resolution of the acoustic absorption and sound speed. We anticipate that this information will aid significantly in the detection of vulnerable plaque.

We will consider two modes of operation for a cylindrical IVUS probe. The first will use a single element probe to both transmit and receive (monostatic mode). The probe needs to be rotated to capture a 360° view. The second will consist of an array where we will transmit on one element and receive an all the elements (multistatic). In both cases we will reconstruct the structure of the tissue by using diffraction tomography principles on the received data

An alternate IVUS imaging paradigm that shows promise in being able to classify plaque is elastography [11, 12]. The contrast in elastic properties between the lipid pool and fibrous cap is quite strong. The elastic properties of the vessel wall can be obtained by observing the deformation of the vessel due to an external pressure. The change in the arterial pressure due to the pumping action of the heart produces measurable deformation of the tissue around the vessel. This deformation can be measured by tracking the motion of patterns in successive IVUS B-scan images. By knowing the arterial pressure and the measured deformation, it is possible to recover the elastic properties of the

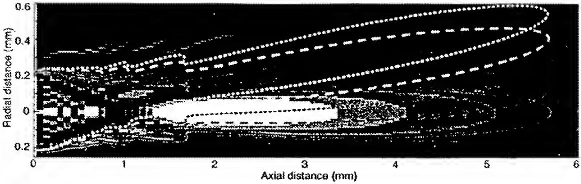

Figure 4: *The acoustic field generated by the Boston Scientific 40 MHz IVUS transducer. The solid line is the -6 dB contour of the pressure field. The dashed lines indicate the -6 dB contours for successive image lines (1.4 degree rotation per line). Note there is significant overlap between image lines which will provide the multiple views of the tissue which is necessary for diffraction tomography.*

tissue. From the elastic properties one can predict plaque composition. The material properties recovered by elasticity are different to what shall be obtained by RRDT. One of our CenSSIS colleagues is investigating elasticity imaging and we plan to implement "information fusion" between the two modalities so that predictions will be based on a greater variety of tissue characteristics. Further, we note that the elasticity images are currently derived from B-scan data could be determined from successive images obtained by any imaging modality. We plan to investigate whether elastography based on RRDT images can lead to improvements in the performance of elastography. Although, the high frame rate required by elastography may make this impractical in a clinical setting.

3.1 Diverse Problems, Similar Solutions

A related non-medical application in which LLNL has a great interest is that of bore-hole imaging to determine the state and location of buried wastes, and the tracking of plumes of underground contaminants as shown in Figure 5. The geometry is identical to that of RRDT IVUS in that a cylindrical probe inserted into a borehole is similar to that of a catheter into an artery. We anticipate that the algorithms and technology developed in IVUS will transport easily across to the problem of borehole tomography.

The newly-constructed CenSSIS SoilBED controlled testbed facility was designed for cross borehole radio frequency tomography. Extending its capability with RRDT will make SoilBED even more effective. Once the RRDT algorithm has been developed as part of this project, we will port it across to the SoilBED facility where it will be used to attack the problem of identifying contaminants in the ground. This project has the potential to provide important advances in other thrusts of the CenSSIS ERC.

4 Research Plan

The research plan consists of three parallel tracks with the common goal of RRDT IVUS algorithm validation and tissue classification. The tracks are *Numerical Studies*, *Scale Model Phantoms*, and *In Vitro Tissue Experiments* as indicated in the flow chart of Figure 6. The summarized track descriptions are the following:

- *In vitro* tissue pathology samples will be analyzed using a scanning acoustic microscope (SAM) to determine their sound speed and absorption properties. Histological analysis will identify the tissue types. By combining these results, we will develop a mapping from observed acoustic properties to tissue types. This will permit us to classify tissues based upon observed acoustic results. The tissue characterization will be used to develop the numerical and tissue mimic phantoms used in the numerical simulations and laboratory scaled IVUS tracks, respectively. Once RRDT has been implemented, and phantom studies completed, experiments on *in vitro* tissue

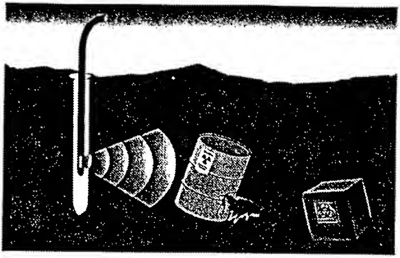

Figure 5: *Application of RRDT bore-hole tomography which demonstrates the similar radial reflection geometry as IVUS.*

samples using a Boston Scientific IVUS system will be used to collect radial reflection mode data to be used in the RRDT IVUS inversion algorithm.

- **Numerical** The numerical simulations will model full acoustic wave propagation under tightly controlled (numerical) experiments. They will generate numerical radial reflection mode data to be used in the RRDT IVUS inversion algorithm.

- **Phantoms** Scale model tissue mimic phantoms will be developed using the results of the tissue characterization. They will be used in controlled, scaled IVUS experiments to generate experimental radial reflection mode data to be used in the RRDT IVUS inversion algorithm.

The results of each of these tracks are reconstructed images of tissue sound speed and absorption. The quality of the images will be validated using the numerical phantoms, tissue mimic phantoms, and *in vitro* tissue samples. The images will be characterized and their components identified (classified as stable plaque, vulnerable plaque, lipid pool, etc.) using the tissue characterization results.

Common to all of the tracks is the development of an efficient, robust inversion scheme for RRDT IVUS. The forward RRDT IVUS model will be validated and analyzed for accuracy using the knowledge gained from the numerical and experimental components.

4.1 *In Vitro* Tissue

Precise characterization of the acoustic properties of the various components of arterial plaque and healthy arterial wall media is necessary for the predictions of sound speed and absorption to be converted into tissue pathology. In addition this information will be used to optimize the RRDT inversion process and to develop realistic input parameters for the numerical, and tissue mimic phantoms.

The acoustic characterization of plaque type has focused mostly on measuring spatially-averaged acoustic backscatter, absorption and sound speed [6, 13, 14] and elastic properties [11]. These are the parameters that are most important for B-scan and elastography respectively. The RRDT modality will provide spatially localized information on the sound speed and absorption of the tissue. It is therefore necessary to develop a spatial database mapping process that will allow us to correlate sound speed and absorption with tissue type.

These data will be used extensively in the rest of the project. They will be used to provide realistic input parameters for the numerical modeling task, which in turn will allow us to determine the operating parameters necessary for RRDT to classify plaque successfully. They will also be used to develop artificial tissue phantoms in the lab with acoustic

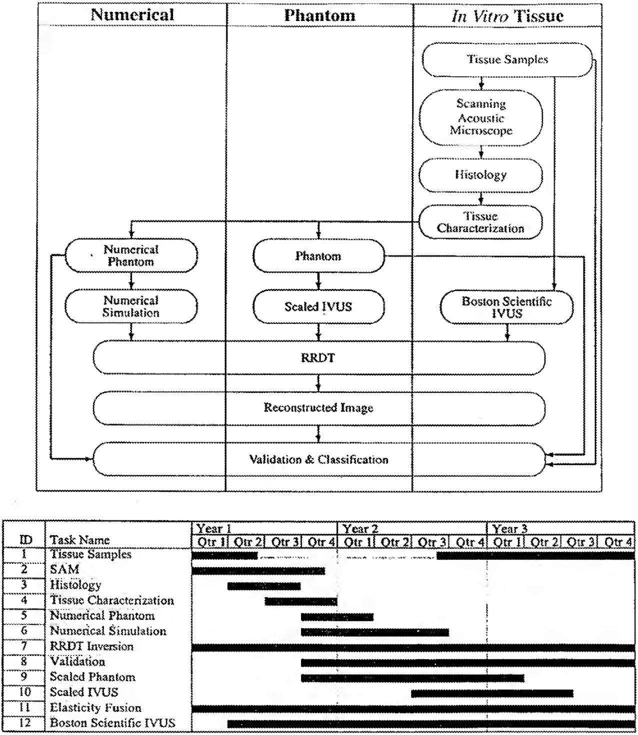

Figure 6: *RRDT IVUS project development flow chart and time line.*

properties similar to that in real vessels. Finally, they will be the crucial data that will allow the predictions of sound speed and absorption by RRDT be converted into tissue pathology

In vitro tissue samples will be provided through a collaboration with CIMIT. The vessels will be cut axially and unrolled to produce a flat sample. Vessels will be selected to contain various types of pathology. We anticipate measuring at least 15 different vessels samples: 5 healthy, 5 with thin cap plaque, and 5 with thick cap plaque.

The ultrasonic properties of the plaques will be measured at the MedBED facility at Boston University using acoustic microscopy. A scanning acoustic microscope (SAM) will be developed, based around a high-frequency pulse-receiver (Panametrics 5910PR) using either a 75 MHz (20 μm wavelength) or 150 MHz (10 μm) focused ultrasound source. The transducers each have a focal spot size on the order of a wavelength. Each tissue sample will be scanned with approximately 5 μm spatial resolution. At each location an ultrasonic pulse will be used to interrogate the sample and the echo data (RF A-line) acquired and stored. To take advantage of the wide bandwidth of the transducers and instruments, a broadband spectroscopy method will be used to make the measurements [15, 16, 17]. The earlier through transmission methods for homogeneous large objects will be modified and extended to a reflection mode for more heterogeneous structures. Data for each RF A-line will undergo signal processing, including the use of a time causal model for viscoelastic materials [15, 17], to produce several key parameters related to absorption and velocity over a broad bandwidth. The resulting parameters can be combined with other line data to map out a quantitative three dimensional image of the structure which can also be visualized in MATLAB. Mathworks, creator of MATLAB, is also a CenSSIS partner. By combining quantitative analysis with 3D imaging, we hope to identify differences in extended plaque structures which would be missed in planar views.

After acoustic measurements, the samples will be returned to the CIMIT team to undergo a histological examination. The samples would be stained so that a complete 3D map of the biological characteristics can be determined. This data will be correlated with the 3D map of the acoustic measurements to create a data-base which relates sound speed and absorption with pathology.

4.2 Numerical Phantom and Simulation

It will be necessary to develop numerical models that can be used to evaluate the performance of RRDT in an idealized and controlled environment. Scanning acoustic microscope data will be evaluated to create typical plaque geometries which will serve as numerical phantom models. The numerical models will then generate synthetic ultrasound data that will be inverted by the RRDT process.

We propose using the following wave equation which is an accurate model of sound propagation and is valid for a fluid with arbitrary inhomogeneities and thermoviscous absorption [18],

$$\nabla^2 p(\mathbf{r},t) - \frac{1}{c^2(\mathbf{r})}\partial_t^2 p(\mathbf{r},t) + \frac{\delta_{TV}(\mathbf{r})}{\rho(\mathbf{r})c^4(\mathbf{r})}\partial_t^3 p(\mathbf{r},t) - \frac{\nabla\rho(\mathbf{r})}{\rho(\mathbf{r})} \cdot \nabla p(\mathbf{r},t) \;=\; -q(\mathbf{r},t), \tag{1}$$

Here $p(\mathbf{r},t)$ is the acoustic pressure, $q(\mathbf{r},t)$ the source, $\rho(\mathbf{r})$ the density of the medium, $c(\mathbf{r})$ is the sound speed of the medium and $\delta_{TV}(\mathbf{r})$ is the acoustic diffusivity. The diffusivity accounts for both thermal and viscous losses in the fluid, and is related to the acoustic absorption coefficient, $\alpha(\mathbf{r})$, via

$$\delta_{TV}(\mathbf{r}) \;=\; 2\,\frac{\alpha(\mathbf{r})c^3(\mathbf{r})}{\omega^2}, \tag{2}$$

where ω is the temporal angular frequency. In contrast to the approximations to be used within the RRDT inversion algorithm model, the numerical simulations will model the full wave equation of Eqn. 1. Time domain simulations will be conducted at both Boston University and Lawrence Livermore National Laboratory.

At BU, the 2D numerical solution of the wave equation is accomplished using the finite-difference time-domain (FDTD) method [18]. The partial derivatives in Eqn. 1 were discretized to second order accuracy in time and fourth order accuracy in space. A perfectly matched layer (PML) is implemented in a region at the edge of the computational domain to reduce reflection artifacts from the numerical boundary. All of the material properties can have arbitrary variation in space, and dispersive media can be modeled.

The collaboration with LLNL will provide access to E3D and A3D, fully three-dimensional elastic and acoustic full field solvers, respectively. E3D/A3D are explicit 2- or 3D elastic/acoustic finite-difference wave propagation codes used for the modeling of seismic/acoustic waves. They are fourth-order accurate in space and second-order accurate in time. They are based on the elastodynamic formulation of the wave equation on a staggered grid. The grid is staggered

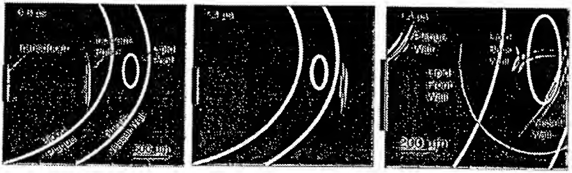

Figure 7: *Snap-shots from a simulation of an ultrasound pulse from a Boston-Scientific probe in a blood vessel with a small lipid-sized occlusion in a plaque-like deposit that has grown on the inside of a vessel wall. The two left frames show the incident pulse passing through the plaque and vessel wall — notice that very little signal is reflected by the components. The right hand figure shows a magnified and intensified view taken at the same time instant as the second frame, so that reflections can be identified. Discrete reflections from individual interfaces are identified. Note that these reflections are scattered in different directions and indicate that an array transducer may collect more signal information and hence produce better images.*

in both space and time. It is regularly spaced, except for the static grid refinement option. The computed variables at each node are the velocities and the components of the stress tensor.

The three-dimensional codes will incorporate the full diffraction and spreading, however, we anticipate that they will also incur a significant computational cost. We will run comparisons between the 2D and 3D codes to evaluate which code produces usable data in the most efficient manner. In particular, we shall determine whether the extra overhead of solving in three dimensions is necessary for this problem.

Simulations of the IVUS problem will be carried out with the numerical models. The data used in this study for the tissue parameters will use both data in the literature, for example, Goss, *et al.* [19], and the data that will be measured by us with the SAM. We will be able to simulate various pathologies using the numerical models. For example, in Figure 7 we show images from a simulation using the BU FDTD code of an IVUS scenario. The model configuration was for the Boston Scientific probe whose typical beam pattern is given in Figure 4, placed within blood vessel with plaque and a lipid pool. The snap-shots of the sound field demonstrate the interaction of the acoustic wave with the different components of the vessel wall. The predicted backscatter data from the codes will be used as an input to the RRDT inversion routine and used to evaluate the performance of RRDT.

4.3 Development of Radial Reflection Diffraction Tomography Inversion Algorithm

In intravascular ultrasound (IVUS), a single transducer rotates at a fixed radius about the center of the probe. At each angular location, the transducer launches a pulse into the medium, in this case, the artery, and collects the returned backscattered field. This is known as a multimonostatic operating mode.[1] Current IVUS imaging techniques rely upon a straight-ray model of sound propagation [20, 21]. That is, the sound waves travel in straight lines subject only to reflection, material absorption, and geometrical spreading due to distance traveled.[2] Variants of the model may or may not take into account refraction, that is, the bending of rays at interfaces, and none account for the wave nature of diffraction. The reconstructed images, formed from the magnitude of the backscattered returns, show only attenuation[3] maps of the medium.

We propose using a wave-based model, diffraction tomography (DT), which more accurately models the wave nature of the sound propagation. Since DT algorithms make use of both the magnitude and phase of the backscattered

[1] An alternative design would be an array of fixed transducers located on an annulus. This would constitute either a bistatic or multibistatic operating mode, depending upon the configuration.

[2] This is also known as "$1/r$" attenuation.

[3] That is, amplitude loss due to the combined effects of absorption, reflection, and refraction

returns, the reconstructions are complex quantities representing the sound speed and absorption of the medium.

Although DT has been applied to various medical imaging problems, for examples see [22, 23], the technique has never been applied to the IVUS outwardly directed radial geometry operating in a reflection mode. A DT inversion algorithm for this geometry, that is, a radial reflection diffraction tomography (RRDT), algorithm has never been developed.

The goal of any DT algorithm is to invert the forward wave-based model. There are problems, however, in inverting the full wave equation of Eqn. 1 for the two unknown parameters of sound speed, $c(\mathbf{r})$, and absorption, $\alpha(\mathbf{r})$, because the density, $\rho(\mathbf{r})$, appears as a spatially varying quantity. We must simplify the full forward model of Eqn. 1. The simplification arises from the fact the tissue density does not vary significantly. That is, there is negligible density variation across tissue types. With this simplification, the $\nabla\rho(\mathbf{r})$ is identically zero and Eqn. 1 reduces to

$$\left[\nabla^2 - \frac{1}{c^2(\mathbf{r})}\partial_t^2 + \frac{\delta_{TV}(\mathbf{r})}{\rho_0 c^4(\mathbf{r})}\partial_t^3\right] p(\mathbf{r},t) = -q(\mathbf{r},t), \tag{3}$$

where we have replaced $\rho(\mathbf{r})$ with a uniform background density ρ_0.

Fourier transforming Eqn. 3 in time, we achieve the Helmholtz equation,

$$\left[\nabla^2 + k^2(\mathbf{r})\right] p(\mathbf{r},\omega) = -q(\mathbf{r},\omega), \tag{4}$$

where ω is the temporal frequency, and the complex wavenumber distribution is defined in terms of the absorption,

$$k^2(\mathbf{r}) \equiv \frac{\omega^2}{c^2(\mathbf{r})} - i\,\frac{2\alpha(\mathbf{r})\omega}{\rho_0 c(\mathbf{r})}, \tag{5}$$

where, in tissue, the absorption increases linearly with frequency, that is, $\alpha(\mathbf{r}) \approx \alpha_0(\mathbf{r})\omega$. It is convenient to express Eqn. 4 in a form in which the inhomogeneity appears on the right hand side. We do so by adding $k_0^2(\omega)p(\mathbf{r},\omega)$ to sides of the equation and moving the $k^2(\mathbf{r})p(\mathbf{r},\omega)$ inhomogeneity to the right hand side:

$$\left[\nabla^2 + k_0^2(\omega)\right] p(\mathbf{r},\omega) = -q(\mathbf{r},\omega) - k_0^2(\omega)\, o(\mathbf{r})\, p(\mathbf{r},\omega). \tag{6}$$

where the *background* wavenumber is $k_0(\omega) \equiv \omega/c_0$ and the *object distribution function* is $o(\mathbf{r}) \equiv k^2(\mathbf{r})/k_0^2(\omega) - 1$. We note that we have expressed the object distribution as being independent of frequency, that is, dispersionless. We show this by substituting Eqn. 5 into the definition of the object distribution function. After simplification, we find

$$o(\mathbf{r}) = n^2(\mathbf{r}) - 1 - i\,\frac{2\alpha_0(\mathbf{r})n(\mathbf{r})c_0}{\rho_0}, \tag{7}$$

where $n(\mathbf{r}) \equiv c_0/c(\mathbf{r})$ is the *index of refraction*. Thus, as long as medium's sound speed and density are independent of frequency[4], so is the object distribution. This is not only a valid assumption [17], but essential to the final inversion algorithm as explained below. In practice, the reconstructed sound speed and absorption distributions represent values averaged over the insonifying frequency bandwidth.

Eqn. 6 is no easier to solve than Eqn. 4, however it "appears" easier in that the left hand side contains no spatial inhomogeneities. The right hand side appears to have two source terms: a *primary* source term, $q(\mathbf{r},\omega)$; and a *secondary* source term given by $k_0^2(\omega)o(\mathbf{r})p(\mathbf{r},\omega)$.

Using Green's Theorem [24, 25], we convert Eqn. 6 from a differential to an integral equation:

$$p(\mathbf{r},\omega) = \int d\mathbf{r}'\, G(\mathbf{r}-\mathbf{r}',\omega)\, q(\mathbf{r}',\omega) + k_0^2(\omega)\int d\mathbf{r}'\, G(\mathbf{r}-\mathbf{r}',\omega)\, o(\mathbf{r}')\, p(\mathbf{r}',\omega), \tag{8}$$

where $G(\mathbf{r},\omega)$ is the free space Green's function,

$$G(\mathbf{r}-\mathbf{r}',\omega) = \frac{e^{ik_0(\omega)|\mathbf{r}-\mathbf{r}'|}}{4\pi\,|\mathbf{r}-\mathbf{r}'|}.$$

[4]or slowly varying with frequency

We observe that the total field is the sum of two components. The first term on the right hand side is defined as the *incident* or insonifying field, $p_i(\mathbf{r},\omega)$. An example of the incident field distribution is shown in Figure 4. The *scattered* field is thus

$$p_s(\mathbf{r},\omega) \;=\; k_0^2(\omega) \int d\mathbf{r}'\, G(\mathbf{r}-\mathbf{r}',\omega)\, o(\mathbf{r}')\, p(\mathbf{r}',\omega). \tag{9}$$

When we evaluate Eqn. 9 at a set of receivers or receiver locations, we obtain an integral relationship between the known measured scattered field, $p(\mathbf{r},\omega)$, and the unknown object distribution, $o(\mathbf{r})$.

Eqn. 9, however, is very difficult to solve as the scattered field, $p_s(\mathbf{r},\omega)$ appears on both sides of the equation, entering implicitly as part of the total field, $p(\mathbf{r},\omega)$. We simplify the problem by taking advantage of the physical fact the acoustic properties of the insonified tissue vary little from the background (assumed to be water). Mathematically, we express this as $k(\mathbf{r}) \approx k_0(\omega)$; a reasonable assumption as indicated in the second frame of Figure 7.

The implication is that we may neglect the scattered field term within the integral and replace the total field by the incident field. This is known as the *Born approximation*. We then express the scattered field as

$$p_s(\mathbf{r},\omega) \approx p_s^B(\mathbf{r},\omega) \;=\; k_0^2(\omega) \int d\mathbf{r}'\, G(\mathbf{r}-\mathbf{r}',\omega)\, o(\mathbf{r}')\, p_i(\mathbf{r}',\omega), \tag{10}$$

where the B superscript indicates we are operating under the Born approximation.

We now consider the geometry of an IVUS scan shown in Figure 2 (b) and specialize Eqn. 10 to the case of a single rotating transducer which launches a pulse and collects the backscattered data at discrete angular locations. The transducer is located at the fixed radius of R_0. Its angle of rotation is θ. Vectorially, we indicate the transducer location and observer points as $\mathbf{r}_0 = R_0\ (\cos\theta, \sin\theta)$ and $\mathbf{r}' = r'\ (\cos\theta', \sin\theta')$, respectively. With this notation, Eqn. 10 reads

$$\boxed{p_s^B(\mathbf{r}_0,\omega) \;=\; k_0^2(\omega) \int_{R_0}^{\infty} r'dr' \int_0^{2\pi} d\theta'\, G(\mathbf{r}_0-\mathbf{r}',\omega)\, o(\mathbf{r}')\, p_i(\mathbf{r}',\omega).} \tag{11}$$

Eqn. 11 is our forward IVUS imaging model. It represents a mathematical mapping of the object distribution from the (r',θ') object space to the (θ,ω) measurement space. In operator notation, we express this as

$$p_s^B(\theta,\omega) \;=\; \mathcal{K}(\theta,\omega;r',\theta')\, o(r',\theta'), \tag{12}$$

where the *forward scattering operator*, $\mathcal{K}(\theta,\omega;r',\theta')$ is defined as

$$\mathcal{K}(\theta,\omega;r',\theta')[\,\cdot\,] \;\equiv\; k_0^2(\omega) \int_{R_0}^{\infty} r'dr' \int_0^{2\pi} d\theta'\, G(\mathbf{r}_0-\mathbf{r}',\omega)\, p_i(\mathbf{r}',\omega)\, [\,\cdot\,]. \tag{13}$$

Eqn. 11, or equivalently Eqn. 12, is the equation we propose to invert for RRDT imaging whether IVUS or borehole related; whether monostatic or bistatic. $p_s^B(\theta,\omega)$ is the known measured scattered field at the transducer at angular location θ and frequency ω. Thus, in operator notation, we may solve Eqn. 12 for the unknown object distribution via

$$o(r',\theta') \;=\; \mathcal{K}^{-1}(\theta,\omega;r',\theta')\, p_s^B(\theta,\omega). \tag{14}$$

The inversion algorithm will determine an expression for $\mathcal{K}^{-1}(\theta,\omega;r',\theta')$, a mapping from the (θ,ω) measurement space back to the (r',θ') object space. This inverse mapping operator will involve integration over temporal frequency variable, ω, and the angular observation variable, θ, to recover the two object spatial variables (r',θ'). It will recover the two-dimensional complex object distribution, $o(\mathbf{r}')$, from which we can obtain the sound speed and absorption through Eqn. 5.

Considering the operator notation of Eqn. 12, it becomes clear why the object distribution must be dispersionless. Our goal is to reconstruct a two-dimensional object. The forward operators maps the object from a two-dimensional space to another two-dimensional space. Thus, we have a sufficient number of free, independent variables to derive an inverse mapping [26]. If the object distribution were a function of frequency as well, the forward mapping would represent a type of projection operator from the three-dimensional (r',θ',ω) space to the two-dimensional (r,ω) space and we would have an insufficient number of free variables to develop and perform the inverse mapping.

In developing the inversion algorithm, we will invert the model for two differing operating modes: monostatic and bistatic. In the former case, the transmitting and receiving transducer are co-located, while in the latter, they are separate and independent. We believe an analytic inverse is possible in both operating modes. Should this not be the case, we intend to develop a numerical inverse based upon a moment method expansion of the object distribution.

4.4 Reconstructed Images and Validation

The images reconstructed by the RRDT algorithm will be compared to the actual input acoustic data and their corresponding histological maps for validation and classification. We will first evaluate the performance off RRDT when used to invert signals from numerical models and scaled experimental models. The performance of RRDT can then be evaluated in a controlled environment. At this stage, different monostatic and bistatic transducer geometries can be evaluated in order to determine the best and most practical option to implement.

4.4.1 Numerical Validation

Two aspects that will be investigated are the assumptions by the RRDT algorithm of uniform density and Born scattering. We anticipate there will be some small variation in density throughout the tissue. The impact on the inversion algorithm will be determined through numerical modeling. Simulations will be run with and without density inhomogeneities and use both sets of data as the input to the RRDT inversion algorithm. Variations in the predictions of the RRDT inversion will be used to estimate the impact of inhomogeneities on RRDT imaging. Similarly, the Born approximation can be tested by numerically increasing the contrast between tissue elements in the simulations until the RRDT no longer provides acceptable performance.

4.4.2 Frequency-Scaled Validation

The RRDT inversion scheme will be experimentally validated with well characterized tissue phantoms. The phantoms will be fabricated to mimic the characteristics of blood vessels including plaque. Ultrasound measurements will be analyzed with RRDT to recover the spatial distribution of these properties. The results from RRDT will be compared to the actual distributions in the phantom.

Preliminary experiments will be carried out using a scaled up model of the vascular problem. The current MedBED facility at Boston University will be augmented with equipment specialized for the IVUS application. A two-axis rotational stage will be installed for independent manipulation of source and receiver. We envision using phantom vessels about 20 times larger than a real vessel — approximately 50 to 100 mm in diameter. The group at BU has substantial experience fabricating and characterizing ultrasound tissue phantoms using agar based tissue phantoms that have been described in the literature [27]. The use of scaled models has been used previously in IVUS experiments [5, 27]. We note that this scaled experiment will be about 50 times smaller than the buried contaminant problem that is also of interest to LLNL which has a length scale 5 m.

The first targets will be simple cylindrical tubes with varying thicknesses and acoustic mismatch. This will allow us to quantify the accuracy and resolution of the inversion technique. Subsequently, we shall create *in vitro* phantoms with an inhomogeneous nature similar to real vessels with plaque — as determined by the SAM measurements. The phantoms are easily cast in layers. Therefore we can create the layered structure similar to that of a vessel. We can also pre-cast small inclusions which can be incorporated into the vessel walls - similar to lipid pools. By adjusting the parameters of the tissue recipe it is possible to independently control both the sound speed and the absorption of each layer. Therefore we can create a well-defined and stable scaled mimic of a vessel wall.

The impact of scaling the diameter of the vessel up by a factor of 20 means that the frequency needs to be scaled down by the same amount. We propose to use 2 MHz circular piston transducers with a diameter of about 10 mm (similar to the Boston Scientific IVUS probe but scaled in size). We will be able to use off-the-shelf probes in the scale experiment. The first experiments will evaluate the performance of two imaging scenarios:

Monostatic A single probe will be used for pulsing and receiving. It will be rotated around and individual radial lines collected. This is identical to the imaging modality used by the single element probe that Boston Scientific will supply.

Bistatic Two transducers will be placed on a common axis. We will pulse with one transducer and receive with the second. The pulsing transducer will be held fixed and the receiver rotated through various angles. For each transmit line this mode collects echo data at various angles.

The single element system is simpler and cheaper to manufacture. However, tomographic reconstructions typically work best when there are "multiple views" of the tissue and it may be that there is not enough information to recover the data from a monostatic system. Recall the images from the simulations, Figure 7 which indicated that some of

the scattered field will not be reflected straight back to the transducer. The bistatic mode will capture more of the backscattered field and this extra data may be particularly necessary for the tomographic reconstruction to produce an acceptable image of the tissue.

Data from the experiments will be used to contrast the performance of monostatic and bistatic RRDT in the known tissue phantoms to predict the spatial distribution of the sound speed and absorption. In particular we will be able to create phantoms with varying contrast in sound speed and absorption. These will be used to determine the threshold contrast levels that the inversion can detect.

In addition, the bistatic configuration can be used to simulate an IVUS array probe - some commercial devices use an array. By combining the response of the receiver at various angles it will be possible to generate a synthetic receiving aperture. Because the *in vitro* environment is stationary it will be possible to collect data with complete freedom of choice between the receiver and source angle. This will allow us to evaluate the performance of the inversion process when applied to an array.

The data from the bistatic experiments will be used design a circular array transducer for use in the scale model. It will be made with multiple elements each at 2 MHz. The size and radial distribution will be determined from the bistatic data and simulations. If the proposed collaboration with Analogic develops then we anticipate creating an IVUS array with 64 elements. This array will be connected to the Analogic ultrasound engine to collect data simultaneously on all channels. If we do not obtain access to the Analogic system then we will fabricate a system with eight elements and use an eight channel acquisition system that we have access to at the BU MedBED.

Experiments will be conducted with these phantoms to contrast the behavior of monostatic, bistatic, and array performance in a more realistic scenario. The data will allow us to determine the parameter space where the three transducer configurations are practical for the IVUS problem.

4.5 *In Vitro* Blood Vessel with Plaque Experiments and RRDT Reconstruction

The final test of RRDT will be to characterize the plaque in a blood vessel. The CIMIT group will provide us with intact samples of blood vessels with various pathologies for *in vitro* experiments. We shall use a single element Boston Scientific probe to obtain IVUS data from the real vessels. The acquired data will be processed with RRDT, which will return spatial maps of the sound speed and absorption. This data will be compared to the correlation of acoustic properties and pathology (from the histological assays and SAM measurements) to predict the presence, location, and type of plaque in the vessel.

After ultrasound evaluation the vessels will be returned to CIMIT for histologic evaluation. The RRDT images and the spatial maps provided by the histology will be compared. We will then be able to evaluate the accuracy of the RRDT system.

4.6 Information Fusion with Quantitative Elasticity Imaging

One of the defining characteristics of vulnerable plaque is the presence of a "lipid pool." Mechanically speaking, the difference between a solid and a liquid is the shear stiffness. Quantitative elasticity imaging provides a way to map the distribution of shear stiffness in tissues. Because of the obvious potential utility of high resolution stiffness imaging in vessel walls, many groups are have been actively pursuing various kinds of elasticity/strain imaging using IVUS [28]-[29]. To date, however, nearly all attempts at IVUS based elasticity imaging have been restricted to the generation of qualitative strain images.

Recent work has shown, however, that strain images can give grossly misleading representations of true stiffness distributions [30]. Therefore, in order to get an accurate representation of tissue morphology in this project, we will examine a "quantitative" elastic imaging method. This requires solving for the tissue stiffness from the measured strain distribution. Imaging the elastic properties of tissue requires four components:

1. a way to image the medium during deformation;
2. a way to "impose" a deformation;
3. a method to track points from one frame to the next in order to infer medium displacement and hence strain;
4. the solution of an inverse problem to obtain the stiffness from the measured strain.

[redacted]

IVUS is well suited to (1) and (3) by providing real-time high resolution images of the vessel. They are not motion corrupted or averaged, but rather effectively represent snap-shots of the medium position in time. In terms of imaging blood vessels, as compared to other tissues, we are lucky regarding issue (2): arterial vessels have their own well-characterized and repeatable deformation fields imposed by the pumping of blood through them. Other groups stop after items (1-3), and call the resulting images "elastograms" or "palpograms." We note that these are images of measured strain distributions. They rarely coincide with the true stiffness distributions, except in the simplest of phantoms. Therefore, we shall focus our attentions on step (4): developing quantitative stiffness images. For this last component, number (4), the vessel geometry may be either a blessing or a curse.

Our recent research [30] has shown that the success of being able to reconstruct a stiffness image from a strain image depends crucially on *an independent* characterization of the boundary conditions in the problem. In the vessel, we may be lucky: we have only one real boundary, the vessel wall, which is subjected to the roughly the same pressure everywhere. This may be sufficient characterization to perform the reconstruction. However, the equations may admit other eigensolutions which are not determined by a knowledge of conditions on the interior boundary alone. Only a detailed analysis of the inverse problem in the cylindrical geometry, akin to that in [30] for rectangular domains, will resolve the issue.

The goal of this part of the proposed project is to develop the tools required to do quantitative elasticity imaging of vessel walls based on IVUS data. To reach the goal, three tasks must be performed. First, an analysis of the inverse problem as just described is needed in order to be determine precisely what data is required for an inversion. Second, an appropriate motion tracking algorithm must be implemented. Finally, an inversion algorithm based on our analysis of the inverse problem must be developed and implemented.

The technical challenges that confront quantitative intravascular stiffness imaging (QISI) are varied. For simple qualitative strain imaging, for example, it suffices to produce a strain picture from which one might conclude that the arterial wall is stiffer on one side than the other. For quantitative imaging, on the other hand, we must go through the exercise of defining precisely what stiffness quantity we are measuring. For initial applications, the quantity will be a stiffness based on linear theory of elasticity and inferred from slow accumulated displacements in diastole. Later, however, we anticipate possibly being able to obtain incremental stiffness values at different points in the cardiac cycle. Our ability to do so will depend to a certain extend on our success in correcting for motion artifacts that tend to plague existing *in vivo* strain imaging techniques [29].

During the cardiac cycle, the IVUS transducer moves substantially within the artery. This impacts conventional elasticity imaging in two significant ways. First, it induces a substantial amount of motion between frames, and so inter-frame correlations can be too low to allow conventional cross-correlation motion tracking to be successful. Second, the "dominant" displacement direction is not necessarily aligned with the A-line of the transducer [31, 32]. To overcome these two difficulties, we shall investigate the use of advanced "elastic" or non-rigid image registration techniques [33, 34, 35, 36, 37]. Such techniques can correct for inter-frame transducer motion and produce accurate measures of the two dimensional displacement field. This one solution, therefore, would seem to solve both problems of transducer motion and "angle corrections." The image registration methods pursued here will benefit from being applied to RRDT images rather than B-scan images. As the RRDT images are anticipated to have fewer artifacts than the corresponding B-scans, the registration and therefore the displacement estimates can be more precise.

QISI images will provide a spatial map (which may even be derived from RRDT) of a third and new tissue parameter: the stiffness. We will "fuse" this data with the two maps of sound speed and absorption to further enhance the imaging capabilities of IVUS.

5 Broader Aspects of Proposed Research

While the proposed research involves novel concepts of ultrasound sensing and imaging, it is represents more than just an academic study. First, it adheres to the spirit of the CenSSIS ERC by integrating the sensor design process and the image reconstruction algorithm. Second, it addresses the needs of the ultimate users of the new technology, including among collaborators both the hospital users and the industrial medical device manufactures. Third, the technology is extendable into a discipline of sensing and imaging totally unrelated to medical applications: underground borehole acoustic sensing. Fourth, the new research makes use of-and adds to-the medical testbed (MedBED) that has been established by CenSSIS, thereby leveraging state of the art modeling, experimental facilities, and expertise of affiliated researchers. And fifth, the computational and scale models proposed provide unique educational discovery opportunities beyond the typical graduate and undergraduate research projects.

In the broadest sense, this project fits in well with the CenSSIS aim to:

1. Advance the technology of sensing and imaging to enable rapid, reliable, and cost-effective identification and assessment of concealed targets; and

2. Help educate a new generation of students in this multidisciplinary state-of-the-art sensing and imaging technology to bring the benefits of this unified approach to challenging technical problems in the next century.

In particular, this intravascular ultrasound diffraction tomography project extends the CenSSIS mission of a unified research and educational discipline of subsurface sensing and imaging which will enable revolutionary systems solutions providing comprehensive, affordable health care. While device manufactures typically work to develop a given sensor for a particular environment, the research herein proposed as part of the CenSSIS ERC seeks to optimize the device in conjunction with the reconstruction algorithm. To form the best high resolution image of the inner walls of the blood vessel to detect the hard to spot vulnerable plaque anamolies, it is not sufficient merely to sense the scattered ultrasound waves within the blood vessel. Instead, it is essential that the device measure and make use of all available information: the phase as well as the magnitude, and to measure it with appropriate speed and focusing. The existing intravascular ultrasound sensors will be continuously reconfigured in a proof-of-concept development test as part of our "end-to-end" optimization strategy all the way from the sensor front-end to the target recognition goal.

The concepts of radial reflection diffraction tomography apply to any sensing problem in which a probe antenna is inserted within a convenient tubular opening. As such, lessons learned from a catheter-based blood vessel sensor can be extended to underground sensing of pollutants or buried solid objects. This is consistent with our concept of promoting a unified discipline to exploit the commonalities that exist among the disparate subsurface imaging problems. This "Diverse Problems, Similar Solutions" strategy is the impetus for changing the present compartmentalized approach to such problems.

The experimental validation of the diffraction tomography theory developed will occur in our MedBED, a laboratory facility where well-characterized environments are studied with versatile, controllable, reconfigurable sensors. This testbed will also serve as an educational resource, allowing students to test their skills in locating concealed objects in a variety of scaled medical environments. MedBED is also a general CenSSIS resource with data available in a standardized form and accessible over the web to test models and algorithms at all the ERC institutions. As with the other CenSSIS testbeds, MedBED will be web-controlled by remote users for research and educational use.

Students working on the scale models and ultrasound devices will learn to address the changing expectations for engineers in the new work force, and connect directly to the current practice and tools of engineering. Our goal is to continue the CenSSIS-sparked systemic change in engineering education. By using this type of cross-disciplinary, real-world challenge we hope to inspire students and infuse them with a systems approach to solving the complex technological/societal problems of the next century.

PATENT

IN THE UNITED STATES PATENT AND TRADEMARK OFFICE

Applicant : Sean K. Lehman

Attorney Docket No.: IL-10883

Serial No. :

Art Unit:

Filed :

Examiner:

For : Radial Reflection Diffraction Tomography

Commissioner for Patents
Alex

EXPRESS MAIL CERTIFICATE

"Express Mail" label number EV283924528US

Date of Deposit March 30, 2004

I hereby certify that the following *attached*

1. Recordation Cover Sheet with Assignment (2 pages)
2. New Application Transmittal (in duplicate)
3. Application (Specification with title page 24 pages, Claims 12 pages, Abstract 1 page)
4. Combined Declaration and Power of Attorney (2 pages)
5. Four (4) sheets of formal drawings
6. Information Disclosure Statement, Form PTO-1449 and 12 US Patents and 12 Other Disclosures
7. Return postcard

is being deposited with the United States Postal Service "Express Mail Post Office to addressee" service under 37 CFR 1.10 on the date indicated above and is addressed to Mail Stop Patent Application, Commissioner for Patents, P.O. Box 1450, Alexandria, VA 22313-1450.

April Masluk
(Type or print name of person mailing paper)

April Masluk
(Signature of person mailing paper or fee)